




Brain proteome profiling implicates the complement and coagulation cascade in multiple system atrophy brain pathology

Rasmus Rydbirk^{1,2,11} · Ole Østergaard³ · Jonas Folke^{1,2} · Casper Hempel^{4,5} · Brian DellaValle^{2,5} · Thomas L. Andresen⁴ · Annemette Løkkegaard^{6,7} · Anne-Mette Hejl⁷ · Matthias Bode⁸ · Morten Blaabjerg⁸ · Mette Møller⁹ · Erik H. Danielsen⁹ · Lisette Salvesen⁷ · Charlotte C. Starhof⁷ · Sara Bech⁷ · Kristian Winge^{7,12} · Jørgen Rungby^{2,10} · Bente Pakkenberg^{1,6} · Tomasz Brudek^{1,2} · Jesper V. Olsen³ · Susana Aznar^{1,2} 

Received: 21 January 2022 / Revised: 12 May 2022 / Accepted: 12 May 2022
© The Author(s), under exclusive licence to Springer Nature Switzerland AG 2022

Abstract

Background Multiple system atrophy (MSA) is a rare, progressive, neurodegenerative disorder presenting glia pathology. Still, disease etiology and pathophysiology are unknown, but neuro-inflammation and vascular disruption may be contributing factors to the disease progression. Here, we performed an ex vivo deep proteome profiling of the prefrontal cortex of MSA patients to reveal disease-relevant molecular neuropathological processes. Observations were validated in plasma and cerebrospinal fluid (CSF) of novel cross-sectional patient cohorts.

Methods Brains from 45 MSA patients and 30 normal controls (CTRLs) were included. Brain samples were homogenized and trypsinized for peptide formation and analyzed by high-performance liquid chromatography tandem mass spectrometry (LC–MS/MS). Results were supplemented by western blotting, immuno-capture, tissue clearing and 3D imaging, immunohistochemistry and immunofluorescence. Subsequent measurements of glial fibrillary acid protein (GFAP) and neurofilament light chain (NFL) levels were performed by immunoblotting in plasma of 20 MSA patients and 20 CTRLs. Finally, we performed a proteome profiling of 144 CSF samples from MSA and CTRLs, as well as other parkinsonian disorders. Data were analyzed using relevant parametric and non-parametric two-sample tests or linear regression tests followed by post hoc tests corrected for multiple testing. Additionally, high-throughput bioinformatic analyses were applied.

Results We quantified more than 4,000 proteins across samples and identified 49 differentially expressed proteins with significantly different abundances in MSA patients compared with CTRLs. Pathway analyses showed enrichment of processes related to fibrinolysis and complement cascade activation. Increased fibrinogen subunit β (FGB) protein levels were further verified, and we identified an enriched recognition of FGB by IgGs as well as intra-parenchymal accumulation around blood vessels. We corroborated blood–brain barrier leakage by a significant increase in GFAP and NFL plasma levels in MSA patients that correlated to disease severity and/or duration. Proteome profiling of CSF samples acquired during the disease course, confirmed increased total fibrinogen levels and immune-related components in the soluble fraction of MSA patients. This was also true for the other atypical parkinsonian disorders, dementia with Lewy bodies and progressive supra-nuclear palsy, but not for Parkinson's disease patients.

Conclusion Our results implicate activation of the fibrinolytic cascade and immune system in the brain as contributing factors in MSA associated with a more severe disease course.

Keywords Movement disorder · Proteomics · Atypical parkinsonism · Fibrinogen · Coagulation factors · Neuro-inflammation · Blood–brain barrier

Abbreviations

AD	Alzheimer's disease
BA9	Broadmann area 9
BBB	Blood–brain barrier
CSF	Cerebrospinal fluid
CTRLs	Controls
DIA	Data-independent acquisition

Rasmus Rydbirk, Ole Østergaard have contributed equally.

Jesper V. Olsen, Susana Aznar have joint senior authorship.

Extended author information available on the last page of the article

DLB	Dementia with Lewy bodies
FGA	Fibrinogen subunit α
FGB	Fibrinogen subunit β
FGG	Fibrinogen subunit γ
GFAP	Glial fibrillary acid protein
HP	Haptoglobin
Igs	Immunoglobulins
LC–MS/MS	Liquid chromatography–tandem mass spectrometry
MS	Mass spectrometry
MSA	Multiple system atrophy
NFL	Neuro-filament light chain
PD	Parkinson's disease
PMI	Post-mortem interval
PSP	Progressive supra-nuclear palsy
PTMs	Post-translational modifications
SAM	Significance analysis of microarrays
scRNA-seq	Single-cell RNA sequencing
α Syn	α -Synuclein

Background

Multiple system atrophy (MSA) is a rare, progressive, neurodegenerative disease. In MSA, most of the brain is affected, including most of the cortical areas [1]. The main pathological hallmark is abnormal accumulation of α -synuclein (α Syn) in oligodendrocytes as glial cytoplasmic inclusions [2]. However, the pathophysiological processes accompanying protein aggregation and neurodegeneration are far from understood.

Post-mortem studies, due to the impossibility to perform molecular studies on brain tissue from living MSA patients, are essential to identify brain-related disease processes that can help us hypothesize on the causative mechanisms behind this disease. Though the temporal sequence of the pathogenic events is still obscure, several causative mechanisms have been proposed, such as α Syn aggregation, cell-to-cell transfer, mitochondria dysfunction and inflammation (reviewed by Monzio Compagnoni and Di Fonzo [2]). Inflammation seems to be an important player in the neurodegenerative cascade in synucleinopathies based on descriptions of neuro-inflammation and infiltration of T cells in preclinical and post-mortem studies [3, 4]. Interestingly, recent studies suggest a direct effect of α Syn pathology on neurovascular unit (NVU) disruption [5, 6]. The NVU is an intricate complex of extracellular and cellular components acting as a functional module in maintaining brain homeostasis through regulation of the blood–brain barrier [7]. Furthermore, the NVU acts as an important component in the communication between the brain and the immune system [8]. Therefore, mapping the molecular pathways associated with NVU disruption can be of importance for

the understanding of the neuro-inflammatory pathophysiology observed in MSA.

Our own observations are in line with a strong neuro-inflammatory condition in MSA, as we have described extended neuronal loss alongside increased numbers of micro- and astroglia [1], elevated cytokine protein levels [9], and gene activation related to innate immune responses [10] in the prefrontal cortex of MSA patients. Recently, we performed an epigenome-wide association study supporting our view of an active immune response in the prefrontal cortex of MSA patients [11]. To extend these observations, we chose to perform a deep bottom-up proteomic profiling in the same brain area. Exploring the proteome in MSA brains allows us to identify highly disturbed protein networks and pathways shedding light on disease-relevant biological processes. Moreover, our aim was to identify aberrant protein changes reflecting pathological events in the brain that are translatable to blood and cerebrospinal fluid (CSF), and may be used as potential indicators for disease severity and/or progression in these types of diseases.

In the present study, we included post-mortem brain tissue samples from the prefrontal cortex of 45 MSA patients and 30 normal controls (CTRLs). We employed nano-flow ultra-high-performance liquid chromatography–tandem mass spectrometry (LC–MS/MS) and validated findings by western blotting, immunohistochemistry, and immunoprecipitation. Further, we assessed protein levels of blood–brain barrier (BBB) permeability markers in plasma samples from a second cohort including 20 MSA patients and 20 CTRLs using immunoblotting. Lastly, we evaluated how our findings in brain tissue were reflected in the CSF by proteome profiling of an independent third cohort consisting of samples from 28 MSA, 20 dementia with Lewy bodies (DLB), 39 progressive supra-nuclear palsy (PSP), and 40 Parkinson's disease (PD) patients as well as 17 CTRLs.

Materials and methods

Human material and sample overview

The human brains utilized in the current study were donated to the Brain Bank at Bispebjerg-Frederiksberg Hospital (Copenhagen University Hospital, Denmark) or to the MRC London Neurodegenerative Diseases Brain Bank (King's College London, United Kingdom). All the donated brains were neuropathologically examined to verify the diagnosis. In total, brains from 30 individuals showing no signs of neuropathological disease and 45 MSA patients were included in cohort 1 (Table 1), individual demographic datum is provided in Table S1. Only donors younger than 80 years of age were included to match age groups. Quality control (QC) samples were generated by pooling equal aliquots

Table 1 Demographics summary of patients and controls

Group	CTRL	MSA	DLB	PSP	PD	P
Brain MS	Brain bank	BBH: 10	KCL: 20	BBH: 22	KCL: 23	—
	Sex	M: 14	F: 16	M: 21	F: 24	—
	Age (years)	68.1 ± 7.9		66.1 ± 5.7		0.236
	PMI (hours)	40.0 ± 19.4		42.8 ± 25.6		1.000
	Disease duration (years)	—		6.6 ± 2.6		—
Brain IHC	Subtype	—		C: 11; Mixed: 2; P: 11		—
	Protein load (mg/ml)	6.9 ± 2.1		6.1 ± 1.7		0.156
	Origin	BBH: 4		BBH: 4		—
	Sex	F: 4		M: 2		0.429
	Age (years)	85.0 ± 11.0		62.0 ± 7.0		0.057
Plasma	PMI (hours)	39.0 ± 23.0		56.0 ± 35.0		0.552
	Disease duration (years)	—		7.0 ± 2.0		—
	Origin	BBH: 20		BBH: 13		0.008
	Sex	M: 10	F: 10	—		1.000
	Age (years)	64.2 ± 7.1		62.3 ± 7.5		0.353
CSF	Disease duration (years)	—		4 ± 2.1		—
	H&Y	—		3.6 ± 1.0		—
	Origin	BBH: 17		BBH: 28		—
	Sex	M: 5	F: 12	M: 12	F: 16	BBH: 20
	Age (years)	56.4 ± 10.6		63.4 ± 7.3		BBH: 39
Summary of the group demographics for samples used for mass spectrometry (MS) or immunohistochemistry (IHC) on brain tissue, plasma samples, or cerebrospinal fluid (CSF) samples utilized in the present study	Time to freeze (min)	57.4 ± 9.3		68.4 ± 13.9		M: 25
	Disease duration (years)	—		5.4 ± 4.0		F: 2
						M: 25
						F: 14
						M: 25

Summary of the group demographics for samples used for mass spectrometry (MS) or immunohistochemistry (IHC) on brain tissue, plasma samples, or cerebrospinal fluid (CSF) samples utilized in the present study

Group differences were assessed using Fisher's exact test (brain bank and sex differences), *t* tests, or ANOVA tests followed by Dunnett's post hoc test against normal, healthy controls (CTRLs) MSA multiple system atrophy, DLB dementia with Lewy bodies, PSP progressive supra-nuclear palsy, PD Parkinson's disease, BBH Brain Bank at Bispebjerg-Frederiksberg Hospital, KCL MRC London Neurodegenerative Diseases Brain Bank at King's College London, M male, F female

Significant differences compared with CTRLs are highlighted in bold and *p*-values indicated in *P*. Mean ± standard deviations are shown for age, post-mortem interval (PMI), protein load, disease duration, Hoehn & Yahr (H&Y) rating, and time to freeze. Age at death is reported for brain samples, whereas age at sampling is reported for plasma or CSF samples

from all samples. Further, 13 replicates were made from 11 samples to test assay variances. For immunohistochemistry, four MSA patients and four CTRLs partly overlapping with cohort 1 were selected, demographic data are given in Table S2. For immunoblotting on blood plasma samples, samples from a second patient cohort (cohort 2, Table 1) consisting of 20 MSA patients and 20 CTRLs were included, demographic data are given in Table S3. Lastly, CSF samples from a third patient cohort comprising 17 CTRLs, and 28 MSA, 20 DLB, 39 PSP, 40 PD patients were included (cohort 3, Table 1), demographic data are given in Table S4. The CSF patient samples were generously donated by the Bispebjerg Movement Disorder Biobank and had been collected as part of the diagnostic assessment.

All experiments were conducted in accordance with the World Medical Association Declaration of Helsinki [12].

Protein extraction of prefrontal cortex proteome

Donated human brains were stored at -80°C . The prefrontal cortex proteome was extracted by transferring ~ 100 mg brain tissue from both gray and white matter to 500 μl Tissue Extraction Reagent II (Invitrogen; #FNN0081) containing 1% (v/v) Protease Inhibitor Cocktail (Sigma-Aldrich; #P8340) in MagNA Lyser Green Beads tubes (Roche; #03,358,941,001) on ice. The tissue samples were disrupted and homogenized at 6 k RPM for 25 s on a MagNA Lyser Instrument (Roche) with cooling for 90 s on an ice rack between runs. Supernatants were transferred to new tubes and spun at $20 \times g$ for 20 min at 4°C . Samples were aliquoted and stored at -80°C until analysis. Protein concentrations were determined by the Bradford method [13]. Protein concentrations did not differ between groups (t test, $p=0.097$), and the coefficient of variation (CV) for protein concentrations for all samples was 30.1%.

In-solution digestion, reduction and alkylation

Protein extracts were centrifuged 5 min at $5 \times g$ to pellet any insoluble material. An aliquot of the supernatant containing 100 μg protein was transferred to a new tube, adjusted to 66 μl , and precipitated by following the first steps of the protein precipitation protocol from a Bio-Rad 2-D clean-up kit (Bio-Rad; #1,632,130). Precipitated protein was re-solubilized in 50 μl 8 M urea supplemented with 5 mM tris(2-carboxyethyl)phosphine (TCEP), 10 mM chloroacetamide (CAA) for reduction and alkylation, respectively. Samples were digested by a two-step procedure by addition of 1 μg endo-Lys C (Wako Pure Chemical Corporation) and incubated for 3 h at 22°C before dilution with 50 mM ammonium bicarbonate to 1 M urea final concentration and continued digestion over night after addition of 2 μg proteomics-grade trypsin (Sigma, # T6567). The digestion was

quenched by addition of 40 μl 10% trifluoroacetic acid (TFA) and the digests were stored at -80°C until further analysis.

Mass spectrometric analysis of prefrontal cortex proteomes

Generated peptides were desalted using SepPak C18 columns (Waters; #WAT054955) activated with 1 ml 100% acetonitrile (ACN) and equilibrated with 3×1 ml 0.1% TFA before loading peptides. Bound peptides were washed on-column with 4×1 ml 0.1% TFA followed by elution with 300 μl 40% ACN before removal of ACN in a Speed-Vac (Thermo Scientific) until the volume was below 50 μl . Before analysis, peptide concentrations were estimated by absorbance at 280 nm measured by a NanoDrop instrument (Thermo Scientific) and peptide concentrations were adjusted to 0.5 $\mu\text{g}/\mu\text{l}$ prior to loading into 96-well plates for sample loading during MS analysis. Samples were loaded onto homemade columns (50 cm long, 75 μm inner diameter) packed with 1.9 μm C18 beads (Dr. Maisch GmbH) using an EASY-nLC 1200 system (Thermo Fisher Scientific). Loaded peptides were separated and eluted into a Q-Exactive HF-X mass spectrometer (Thermo Fisher Scientific) as previously described [14] by applying a 180 min gradient ($t=0$ min: 5% solvent B, $t=120$ min: 29% solvent B, $t=180$ min: 55% solvent B; Solvent A: 0.1% FA; Solvent B: 80% ACN, 0.1% FA) with a flowrate of 250 nl/min. MS data were acquired recording full-scan spectra [300–1500 mass/charge (m/z)] with 120,000 resolution at 400 m/z ; and MS/MS data were recorded at 30,000 resolution in a data-dependent mode fragmenting the 12 most abundant ions (charge state 2 or higher) by higher-energy collision dissociation at 28% normalized collision energy. MS/MS spectra were recorded using dynamic exclusion (30 s) to minimize repeated fragmentation of the same peptides.

Detection of FGB in brain extracts by western blotting

Five μg total protein from brain lysates was loaded onto NuPAGE 4–12% Bis–Tris 15-well SDS-PAGE gels (Invitrogen, #NP0323BOX) and blotted to nitrocellulose membranes after electrophoresis. The membranes were blocked with 5% BSA in PBS-T buffer (PBS with 0.1% Tween 20, pH 7.4) followed by overnight incubation with primary antibodies (FGB: Rabbit anti-human FGB diluted 1:2,000; Sigma Prestige Antibodies, #HPA001901, RRID:AB_10788864). For loading control, Rabbit anti-human GAPDH diluted 1:5,000; Abcam; #ab8245, RRID:AB_2107448). After washing 3X in PBS-T, the membranes were incubated for one hour with an HRP-conjugated secondary antibody (goat anti-rabbit IgG, diluted 1:10,000, Jackson ImmunoResearch; #111–036-045, RRID:AB_2337943) in PBS-T with 5% skim milk before incubation for 2 min with Novex ECL chemiluminescent substrate and recording by exposure of high-performance

chemiluminescence films (Amersham Hyperfilm). After exposure and development in a Kodak Medical X-ray processor (Carestream Health), scanned films were analyzed in ImageJ for band quantification.

Detection of GFAP and NFL in plasma protein by immunoblotting

Blood samples were collected in EDTA–blood monovette tubes from patients and CTRLs from cohort 2 (Table 1). After collection, blood samples were centrifuged at $2 \times g$ for 10 min at 4°C to isolate the plasma fraction before aliquoting and storage at -80°C . Motor severity of the patient was assessed at the time of sampling using the Hoehn & Yahr rating scale [15].

On the day of analysis, 2 μl of plasma was dotted in duplicate onto nylon membranes (Hybond N+; Amersham; #RPN203B) similar to DellaValle, Hasseldam [16] and left to dry. Membranes were blocked in blocking buffer with 5% skim milk in TBS-T (Tris-buffered saline with 0.05% Tween 20) followed by incubation overnight at 4°C in blocking buffer supplemented with primary antibodies (rabbit anti-glia fibrillary acidic protein (GFAP): DAKO; #GA524, RRID:AB_2811722, diluted 1:2,000 or rabbit anti-neurofilament light chain (NFL): Abcam; #ab223343, RRID:AB_2891198, diluted 1:2,000). Membranes were then washed 3X in TBS-T and incubated with blocking buffer supplemented with HRP-conjugated secondary antibody (goat anti-rabbit: DAKO; #P044801, RRID:AB_2617138, diluted 1:5000) for 1 h at room temperature before washing 3X in TBS-T and incubation with SuperSignal Femto Reagent (Thermo Scientific) as described by the manufacturer. Membranes were imaged for chemiluminescence with a CCD camera (GE; LAS 4000) and immunoblots were analyzed with ImageJ [17] for raw integrated density.

Immunocapture

Immune complexes were isolated in triplicate experiments from groupwise pooled brain extracts from the patient cohort 1 using protein G-coupled Dynabeads (Dynabeads Protein G Immunoprecipitation Kit, Invitrogen; #10007D) with minor modifications to the manufacturer's instructions. In brief, 200 μl re-suspended beads were transferred to Eppendorf tubes. Beads were isolated and washed in washing buffer two times using a magnet before addition of 500 μl brain extracts and incubation for 40 min at room temperature with rotation. For control experiments, the beads were first saturated with mouse IgG1 isotype antibody (Agilent Technologies, Inc.; #X093101-2, RRID:AB_2889134, 15 μg antibody per 50 μl beads) in Ab binding and washing buffer by incubation 40 min at room temperature with rotation prior to 3X washing and addition of brain extracts. For both experiments and

control experiments, the supernatants were then removed after 40 min incubation of beads with brain extracts and the beads were washed 3X in washing buffer. Immune complexes were then eluted from the beads by incubation in 60 μl Elution Buffer for 3 min with rotation. Elutions were performed twice per sample, and eluates were transferred to clean tubes and pooled. A negative control sample not exposed to antibody or lysate were also generated. Samples were stored at -80°C until further analysis.

Immunohistochemistry and immunofluorescence

Immunostainings were performed as described previously [9]. In short, brain samples covering both gray and white matter tissue were fixed in 10% formalin buffer for minimum 48 h. Then, samples were embedded in paraffin on a Leica ASP300 S tissue processor (Leica, DEU). Using a vibratome, 5 μm sections were placed on glass slides. Samples were deparaffinized before antigen retrieval by heating in buffer at pH 6 (for FGB, and NeuN) or pH 9 (for GFAP). For light microscopy, a two-step HRP-based immunohistochemical technique was used. The primary antibody (FGB: Rabbit anti-human FGB diluted 1:50; Sigma Prestige Antibodies, #HPA001901, RRID:AB_1078864) was incubated for 1 h in PBS at room temperature. After blocking for endogenous peroxidases with 3% H_2O_2 , slides were incubated with a goat anti-rabbit HRP-conjugated EnVision + complex (DAKO; #K4003, RRID:AB_2630375). Finally, slides were developed by adding 3,3'-diaminobenzidine tetrahydrochloride hydrate (DAB) as a substrate. Once dried, slides were counterstained with Mayer's hematoxylin, and further dehydrated in ethanol before cover-slipped with DPX Mounting Medium (CellPath; #SEA-1304-00A). For double immunofluorescence labeling, slides were prepared using the same approach and then incubated with rabbit anti-human FGB (Sigma Prestige Antibodies, #HPA001901, RRID:AB_1078864, diluted 1:50) together with either a mouse anti-NeuN (Millipore/MERCK, #MAB377, RRID:AB_2298767, diluted 1:500) or a mouse anti-GFAP (DAKO, #MO761, RRID:AB_2109952, diluted 1:50). Slides were incubated overnight at 4°C , and then incubated with AlexaFlourTM488-conjugated goat anti-mouse (ThermoFisher; #A-11029, RRID:AB_2534088, diluted 1:200) and AlexaFlourTM647-conjugated goat anti-rabbit (ThermoFisher; #A-21244, RRID:AB_2535812, diluted 1:500) for 1 h in PBS at room temperature. After washing, slides were cover-slipped with a mounting media with DAPI (Abcam; #ab104139). An Olympus BX60 microscope was used for visualizing the slides. Antibody specificity was verified using isotype controls (mouse IgG; DAKO; #X0931; RRID:AB_2889134; or rabbit IgG; DAKO; #X0936; RRID:AB_577471; data not shown).

Stereological quantification

FGB immunoreactivity was quantified under a light microscope following Cavalieri's point-counting principle as previously described [1]. In short, total slide areas were encircled under a 4× objective on an Olympus microscope while the immunoreactive area was estimated using a 60× objective using the VIS software (Visiopharm) applying Systematic Uniform Random Sampling (SURS). All quantifications were performed by a blinded observer. Points that were superimposed on areas with immunoreactivity were sampled. The immunoreactive area was estimated by multiplication of sum of points to the area per point.

Tissue clearing and 3D imaging

Formalin-fixed tissue blocks, from the prefrontal cortex, were dissected into pieces of approximately 1 × 1 × 1 mm. Tissue clearing was performed using the previously described FLASH protocol [18]. After washing in PBS, tissue blocks were immersed in FLASH retrieval solution 1, containing of 4% SDS in 200 mM borate buffer (Sigma-Aldrich) and incubated for 1 h at room temperature, followed by 12 h at 54 °C. Tissue blocks were washed in PBS supplemented with 0.2% Triton X-100. Tissues were blocked for 24 h at room temperature in 10% goat serum (Gibco), 1% BSA (Sigma-Aldrich), 5% DMSO dissolved in PBS supplemented with 0.2% Triton X-100. Then, primary antibodies were applied diluted in blocking buffer. Tissue blocks were incubated with the primary antibodies for 72 h on an orbital shaker at room temperature. Fibrinogen was detected targeting FGB (rabbit anti-human FGB, RRID:AB_1078864, diluted 1:50; Sigma Prestige Antibodies, #HPA001901), while GFAP was detected using a rabbit anti-GFAP antibody (Dako; #Z0334, RRID:AB_10013382, diluted 1:400). After incubation, blocks were washed three times using PBS supplemented with 0.2% Triton X-100; washing lasted for 24 h. Primary antibodies were detected using Alexa568-conjugated goat anti-rabbit (ThermoFisher: #A-11011). After incubation with secondary antibodies, tissue blocks were washed using PBS supplemented with 0.2% Triton X-100. After washing, tissues were dehydrated in methanol (Sigma-Aldrich) starting at 30%, followed by 50%, 75% and 2 × 100%. Each step lasted for 2–4 h. Ethyl cinnamate (VWR) was used as clearing agent as previously described [19]. Tissue blocks were cleared for a minimum of 6 h at room temperature and imaged right after. Cleared specimens were immersed in ethyl cinnamate and imaged in 8-well Ibidi slides with glass bottom (#1.5; Ibidi GmbH). A Nikon Ti2 spinning disk (CSU W1) confocal microscope was used for image acquisition (Nikon Instruments Inc.). All images were acquired using a 20× objective (NA: 0.75). Fluorophores were excited using a 561 nm laser and detected

using a 600/50 emission filter. Due to depth, a Z-correction was applied ensuring non-saturating acquisition. Fluorescent images were imported into ImageJ and prepared for presentation [20]. Z-stacks saved as AVIs were saved at 10 fps. 3D reconstructions were performed using *napari* [21] using maximum intensity projection-based rendering. Rendering: Isosurface was used for fibrinogen while maximum intensity projection was used to render GFAP.

Analysis of cerebrospinal fluid samples

Upon collection, CSF samples were centrifuged within the first hour after extraction for 10 min at 2 k×g and 4 °C, the supernatant aliquoted and stored at – 80 °C.

Fractionation of cerebrospinal fluid samples

On the day of analysis, samples were thawed on ice and subjected to differential centrifugation to separate samples into fractions containing micro-vesicles, exosomes and genuine soluble proteins. In brief, crude CSF was first centrifuged for 3 min at 600×g to remove any remaining cellular debris or precipitates formed during freezing. The supernatant was then transferred to a new tube followed by centrifugation at 20 k×g for 30 min to pellet micro-vesicles. The supernatant was transferred to a new tube and centrifuged at 120 k×g for 90 min to pellet exosomes before transfer of the genuine soluble proteins to a fourth tube. All pelleted fractions were washed once with PBS before tryptic digestion.

Tryptic digestion of cerebrospinal fluid samples

In brief, the three pelleted fractions were re-suspended in 30 µl GuHCl [6 M Gu–HCl, 100 mM Tris–HCl pH 8.5 supplemented with 5 mM TCEP and 10 mM CAA] and 10 µl from the soluble fraction was mixed with 30 µl GuHCl solution before addition of 0.5 µg endo-Lys C to all tubes. After 2 h digestion at 37 °C, each tube was then supplemented with 150 µl 25 mM Tris–HCl pH 8.5 to dilute the GuHCl to 1 M before addition of 1 µg sequencing grade trypsin (Promega, #V5117) and continued digestion overnight. The digestion was terminated by addition of 10% TFA to 1% TFA final concentration and generated peptides were desalted using homemade StageTips [22].

Mass spectrometry analysis of cerebrospinal fluid samples

For mass spectrometry analysis, 250 ng desalted peptides were loaded via EvoTips onto homemade columns (15 cm long, 150 µm inner diameter) packed with 1.9 µm C18 beads (Dr. Maisch GmbH, #r119.aq.0003) using an Evosep One LC system (Evosep Biosystems). Loaded peptides were separated and eluted into a Q Exactive HF-X mass spectrometer

(Thermo Fisher Scientific) as previously described [23] by applying a 45 min gradient [30 samples per day] using data-independent acquisition (DIA) mode. In brief, full-scan MS1 spectra were recorded in the m/z range 350–1400 Da with the resolution set to 120,000 at m/z 200; AGC target was 3e6 and IT 45 ms. The MS2 scans were recorded in 48 successive 15 Da windows (with 1 Da overlap) starting from 368.5 Da (center of isolation window) recorded at 15,000 resolution; AGC target was 3e6 and IT 22 ms. The normalized collision energy was set to 25% and both MS1 and MS2 spectra were recorded in profile mode.

Data analysis

Raw LC–MS/MS data processing and analysis

Recorded raw files for prefrontal cortex proteomes were analyzed using MaxQuant version 1.6.0.17 [24] for peptide quantitation by MS1 intensity and for protein identification using the built-in Andromeda search engine [25] searching against a modified UniProt database downloaded February 2018, where predicted signal peptides were removed from the protein sequences. In addition, MaxQuant also calculated intensity-based absolute quantification (iBAQ) values [26] for estimating the absolute abundance of different proteins within a single sample.

The MaxQuant analyses were performed with the following settings: Enzyme: Trypsin, and maximum 2 missed cleavage sites. Precursor mass tolerance was 4.5 ppm, and fragment mass tolerance 20 ppm. Variable modifications: Oxidation (M), and acetyl (protein N-terminal). Fixed modifications: Carbamidomethyl (C). Peptide FDR 1%, protein FDR 1%, minimum peptides: 1. Match between runs: 0.7 min. All other settings were left at the default settings. The dataset has been uploaded to the ProteomeXchange Consortium via the PRIDE repository [27]. The data are available via ProteomeXchange with the identifier PXD026370.

Raw files from LC–MS/MS analysis of the CSF samples were searched against a modified SwissProt database (downloaded October 2018), where signal peptides had been removed, using Spectronaut v. 14.7 [28] applying sum of peptides quantified at the MS1 level to report protein quantities. Settings were as follows: Enzyme: Trypsin. Missed cleavages: max 2 missed cleavage sites. Variable modifications: Oxidation (M), and acetyl (protein N-terminal). Fixed modifications: Carbamidomethyl (C). All other settings were left at the default settings. The dataset has been uploaded to the ProteomeXchange Consortium via the PRIDE repository. The data are available via ProteomeXchange with the identifier PXD026802.

All proteins quantified per sample are shown in Table S5. Using SynGO [29], we investigated whether our protocol

allowed for solubilization and detection of synaptic proteins. Indeed, we were able to quantify proteins for 936 out of 1,225 genes included in the SynGO database. SynGO gene ontology analyses of these genes showed significant enrichment for terms related to synapses (Table S6) demonstrating the robustness of our experimental setup.

Clustering and outlier detection

Unsupervised hierarchical clustering showed strong correlations between all QC samples as well as replicate samples, respectively (Fig. S1A). We obtained small variation in protein intensity CVs for both highly and lowly expressed proteins (Fig. S1B). For the replicate samples, one technical replicate per sample was included in the downstream analyses. The unsupervised hierarchical clustering analysis identified a cluster of 11 samples (eight MSA, three CTRLs) separate from the remaining samples. When analyzing the differential expression of these samples against the remaining samples, 1997 proteins showed significant differential expression ($FDR < 0.05$) underlining their relatedness against the remaining samples. Of the significantly different proteins, 1280 were up-regulated while 717 were down-regulated (Table S7). Pathway analyses identified biological pathways related to cell receptor changes (PANTHER) and inflammatory processes (Reactome, GO; Table S8). It is unknown whether this difference was caused by either technical or biological divergence. Based on the distant clustering of the 11 samples and the extreme number of significantly different proteins compared with the remaining samples, we considered these samples as outliers and excluded them from the downstream analyses.

Filtering and testing

Protein intensity values were processed using Perseus v. 1.6.8.0. First, proteins were filtered if flagged for “Potential contaminant”, “Reverse” or “Only identified by site”. Second, proteins that were present in less than 70% of samples in at least one group were removed. Third, data were \log_2 transformed before imputation using values from a normal distribution. Fourth, group differences were considered using t tests, significant differences were determined using a permutation-based FDR calculation with 250 permutations ($FDR = 0.05$, $s_0 = 0.1$).

Binary classifier modeling

A supervised machine learning approach with binary classification was performed to further investigate the strength of the observed group differences in the MS data on brain

lysates. Regression models were evaluated using *caret* [30] in R v. 4.0.3 [31], considering *glmnet*, *random forest*, *kNN*, *support vector machine*, and *naive Bayes* models. For training, 75% of the samples were selected randomly retaining the original group proportions. Testing was performed with 10 iterations per subsampling using 2–4 random sub-samplings (k) on the remaining 25% of the samples.

RNA expression in single cells

For gene expression analysis of proteins of interest in single cells, we used publicly available datasets from the BRAIN Initiative Cell Census Network (BICCN, RRID:SCR_015820; <https://biccn.org/>) available at the Neuroscience Multi-omic Archive (NeMOarchive, RRID:SCR_016152; <https://nemoarchive.org/data/>). Specifically, we investigated human datasets from the primary motor cortex of the frontal cortex. These data included 11,589 nuclei from five donors. Data were aligned to the GRCh38.p2 reference genome using the STAR aligner. Count data were integrated using *pagoda2* [32] and *Conos* [33] in R v. 4.0.3 [31].

Bioinformatics

Pathway analyses were performed using Reactome v. 65 [34], PANTHER v. 14.1 [35], or GO rel. 2019–10–08 [36, 37] databases. Protein–protein network analyses were performed using STRING-db v. 11 [38] and presented using Cytoscape v. 3.8.1 with Omics Visualizer v. 1.3.0 [39]. Data from pull-down experiments were analyzed in R v. 4.0.3 [31]. Adj. *p* values were calculated using the Benjamini–Hochberg correction [40]. Plots were created using *ggplot2* [41].

Results

Sample filtering and data validation

In the present study, we performed shotgun mass spectrometry (MS)-based quantitative proteomics of human brain lysates from the prefrontal cortex of MSA patients and CTRLs. An overview of the experimental workflow is shown in Fig. 1A. We analyzed 30 CTRL and 45 MSA samples along with 14 QC samples and 13 replicates of 11 randomly picked samples as assay controls, in total 102 samples. Combined computational analysis of all 102 samples resulted in the identification of 99,979 unique peptides from 6,074,136 peptide-spectrum matches covering 5,959 proteins at 1% FDR after removal of proteins flagged by MaxQuant as REV (reverse decoy hits) or flagged as “only identified by site”. For the QC samples, focusing on 3,732

proteins detected across all samples, we calculated the mean CV of these protein intensities based on label-free quantitation to 14.8% ($n = 14$). For the 13 replicates, considering all proteins detected within replicates (4042–4324 proteins), we calculated the mean intra-column CVs to 10.0% (range 7.5–12.5%, $n = 2$), and the mean inter-column CVs to 16.0% (range 12.3–22.6%, $n = 9$). After filtering the dataset for proteins quantified in at least 70% of the samples in either the MSA or the CTRL group, 4348 unique proteins remained with a mean of 4216 unique proteins identified per sample (Fig. S1C). We used these proteins and performed supervised machine learning using binary classifier model to investigate how well our two sample groups could be differentiated based on raw protein intensities. Our models showed excellent performance with high accuracy (mean \pm SD 0.863 ± 0.121 to 0.944 ± 0.059 , 10 iterations) and moderate to good distinction between groups (Cohen's κ [42], mean \pm SD 0.594 ± 0.401 to 0.855 ± 0.161 , 10 iterations; Figures S2A–C, Table S9).

Immune system and blood-clotting factors are increased in MSA brains

To identify significantly regulated proteins between the MSA patients and CTRLs, we performed a significance analysis of microarrays (SAM)-based *t* test statistics and applied a threshold of FDR < 0.05 at which 49 proteins presented significantly different abundance levels (Fig. 1B; Table 2). These proteins included immune components, such as immunoglobulins (Igs) and complement factor B (CFB), extracellular matrix components, such as collagen alpha-2(VI) chain (COL6A2), collagen alpha-1 (XIV) chain (COL14A1), olfactomedin-like protein 3 (OLFML3), Pro-largin (PREL) and blood-clotting factors, with plasminogen (PLG), thrombin (F2) and fibrinogen subunits α (FGA), β (FGB) and γ (FGG) being some of the proteins with the most increased levels in the MSA brains. Eight of the significantly different proteins, including FGG, were overrepresented in the binary classifier models (Table S10), thereby highlighting the importance of differential expression of fibrinolysis components in our data. Functional protein interaction analyses showed network formation for 26 of the 31 non-Ig proteins underlining a strong relationship between the significant differentially expressed proteins in MSA brains (Fig. 1C). Biological pathway analyses on the 49 significantly different proteins identified enrichment of pathways related to two processes: Blood clotting (“blood coagulation (P00011)”, adj. $p = 7.46\text{E-}11$, PANTHER; “plasminogen activation cascade (P00050)”, adj. $p = 1.87\text{E-}07$, PANTHER), and immune system activation (e.g., “complement cascade (R-HSA-166658)”, adj. $p = 4.68\text{E-}12$, Reactome; “regulation of complement cascade (R-HSA-977606)”, adj. $p = 7.58\text{E-}2$, Reactome; “humoral immune response

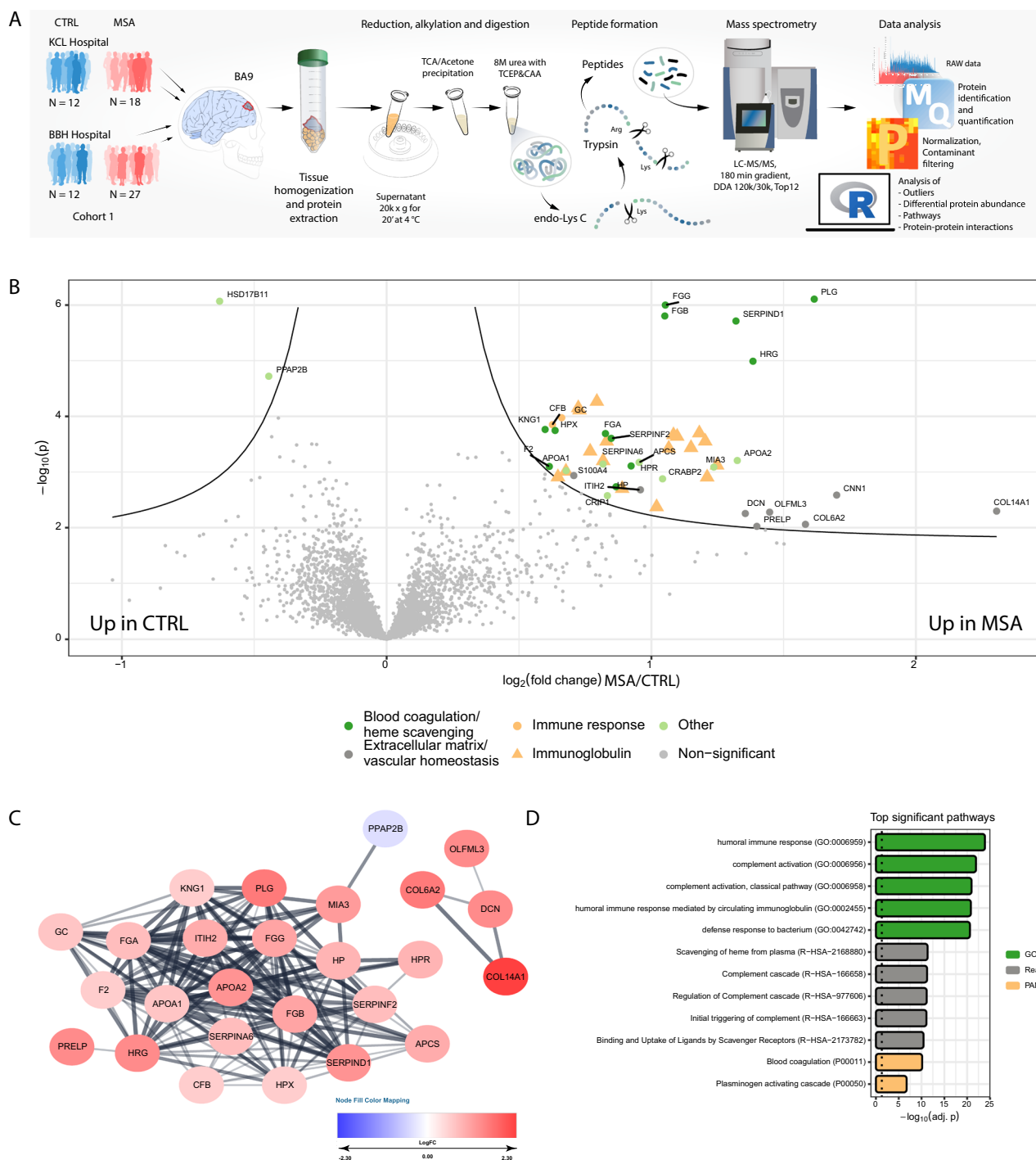


Fig. 1 Overrepresentation of immune and coagulation cascade-related proteins in multiple system atrophy brain tissue. **A** Experimental and data analysis workflows. Brain tissue from Broadmann's area 9 (BA9) were excised from either multiple system atrophy (MSA) patients or normal, healthy controls (CTRLs). Brains from the Bispbjerg Brain Bank (BBH Hospital) and the King's College London Brain Bank (KCL Hospital) were included. Samples were homogenized using ceramic beads and centrifuged before protein precipitation, desalting, and peptide formation by in-solution tryptic digestion and analysis by mass spectrometry. Data were filtered for

reverse hits and contaminants before analysis of quality control (QC) samples and identification of outliers. Eventually, different unbiased analyses were performed. **B** Volcano plot visualizing the proteins showing significantly different abundances between groups. Significant proteins have been annotated with biological functions through manual curation and highlighted. **C** A protein-protein interaction network derived from the STRING database showing relatedness of the non-immunoglobulin proteins highlighted in **(B)**. Red colors indicate up-regulated proteins, blue colors down-regulated proteins. **D** Top significant overrepresented terms from pathway analyses

Table 2 Significantly different proteins from brain extracts identified with mass spectrometry

<i>P</i>	log2(fold change)	Protein ID	Protein name	Gene name
7.83E-07	1.62	P00747	Plasminogen	<i>PLG</i>
8.54E-07	-0.63	Q8NBQ5	Estradiol 17-beta-dehydrogenase 11	<i>HSD17B11</i>
1.00E-06	1.05	P02679	Fibrinogen gamma chain	<i>FGG</i>
1.57E-06	1.05	P02675	Fibrinogen beta chain	<i>FGB</i>
1.94E-06	1.32	P05546	Heparin cofactor 2	<i>SERPIND1</i>
1.02E-05	1.38	P04196	Histidine-rich glycoprotein	<i>HRG</i>
1.90E-05	-0.45	O14495	Lipid phosphate phosphohydrolase 3	<i>PPAP2B</i>
5.42E-05	0.79	P01859	Immunoglobulin heavy constant gamma 2	<i>IGHG2</i>
7.06E-05	0.72	P01834	Immunoglobulin kappa constant	<i>IGKC</i>
7.75E-05	0.73	P01857	Immunoglobulin heavy constant gamma 1	<i>IGHG1</i>
1.06E-04	0.66	P02774	Vitamin D-binding protein	<i>GC</i>
1.41E-04	0.63	B4E1Z4	Complement factor B	<i>CFB</i>
1.72E-04	0.60	P01042	Kininogen-1	<i>KNG1</i>
1.80E-04	0.64	P02790	Hemopexin	<i>HPX</i>
1.99E-04	1.18	A0A0C4DH35	Immunoglobulin heavy variable 3-35	<i>IGHV3-35</i>
2.04E-04	0.83	P02671	Fibrinogen alpha chain	<i>FGA</i>
2.16E-04	1.08	A0A0C4DH31	Immunoglobulin heavy variable 1-18	<i>IGHV1-18</i>
2.30E-04	1.10	P23083	Immunoglobulin heavy variable 1-2	<i>IGHV1-2</i>
2.49E-04	0.85	P08697	Alpha-2-antiplasmin	<i>SERPINF2</i>
2.80E-04	1.20	A0A075B7D0	Immunoglobulin heavy variable 1/OR15-1	<i>IGHV1OR15-1</i>
2.81E-04	0.83	A0A0B4J1X5	Immunoglobulin heavy variable 3-74	<i>IGHV3-74</i>
3.67E-04	1.15	A0A075B7D8	Immunoglobulin heavy variable 3/OR15-7	<i>IGHV3OR15-7</i>
3.76E-04	1.07	P01766	Immunoglobulin heavy variable 3-13	<i>IGHV3-13</i>
4.25E-04	0.77	P01861	Immunoglobulin heavy constant gamma 4	<i>IGHG4</i>
6.22E-04	1.33	P02652	Apolipoprotein A2	<i>APOA2</i>
6.30E-04	0.82	P01780	Immunoglobulin heavy variable 3-48	<i>IGHV3-48</i>
6.72E-04	0.95	P02743	Serum amyloid P-component	<i>APCS</i>
7.21E-04	0.82	P08185	Corticosteroid-binding globulin	<i>SERPINA6</i>
7.56E-04	1.25	A0A0B4J1Y9	Immunoglobulin heavy variable 3-72	<i>IGHV3-72</i>
7.78E-04	0.92	P00739	Haptoglobin-related protein	<i>HPR</i>
7.96E-04	0.61	P00734	Prothrombin	<i>F2</i>
8.16E-04	1.24	Q5JRA6	Melanoma inhibitory activity protein 3	<i>MIA3</i>
9.44E-04	0.68	P02647	Apolipoprotein A1	<i>APOA1</i>
9.72E-04	0.68	A0A0B4J1V1	Immunoglobulin heavy variable 3-21	<i>IGHV3-21</i>
1.16E-03	0.71	P26447	S100 calcium-binding protein A4	<i>S100A4</i>
1.23E-03	0.65	P01762	Immunoglobulin heavy variable 3-11	<i>IGHV3-11</i>
1.24E-03	1.21	P04433	Immunoglobulin kappa variable 3D-11	<i>IGKV3D-11</i>
1.33E-03	1.04	P29373	Cellular retinoic acid-binding protein 2	<i>CRABP2</i>
1.84E-03	0.87	P00738	Haptoglobin	<i>HP</i>
1.99E-03	0.89	P01619	Immunoglobulin kappa variable 3-20	<i>IGKV3-20</i>
2.09E-03	0.96	P19823	Inter-alpha-trypsin inhibitor heavy chain H2	<i>ITIH2</i>
2.60E-03	1.70	P51911	Calponin-1	<i>CNN1</i>
2.66E-03	0.83	P50238	Cysteine-rich protein 1	<i>CRIP1</i>
4.24E-03	1.02	A0A0J9YY99	Immunoglobulin heavy variable 3-30-5	<i>IGHV3-30-5</i>
5.05E-03	2.30	Q05707	Collagen XIV alpha-1 chain	<i>COL14A1</i>
5.27E-03	1.45	Q9NRN5	Olfactomedin-like protein 3	<i>OLFML3</i>
5.57E-03	1.36	P07585	Decorin	<i>DCN</i>
8.72E-03	1.58	P12110	Collagen VI alpha-2 chain	<i>COL6A2</i>
9.48E-03	1.40	P51888	Prolargin	<i>PRELP</i>

Table 2 (continued)

Significantly different proteins for multiple system atrophy patients compared with normal, healthy controls from the mass spectrometric analyses on brain tissue. Protein IDs were extracted from the UniProt database, gene names were extracted from the Ensembl database

(GO:0,006,949)", adj. $p = 1.26\text{E-}24$, GO; "complement activation (GO0006956)", adj. $p = 1.13\text{E-}22$, GO; top significant pathways are shown in Fig. 1D and the full list of significant pathways is reported in Table S11). Additional investigation of the expression of protein targets that have previously shown relevance to MSA disease processes, including αSyn , did not reveal any significant differences between groups (t test, $p > 0.05$; (Fig. S1D).

Single-cell expression of significant proteins

To investigate the intra- or extra-cerebral expression as well as cell type expression of the significantly differential proteins, we mapped their intercellular expression patterns using a public single-cell RNA sequencing dataset. The single-cell RNA sequencing (scRNA-seq) data were generated from samples from the primary motor cortex of the frontal cortex from healthy human subjects. We used known gene markers to annotate cell types (Fig. S3A). A UMAP embedding of the scRNA-seq data showed good distinction between cell types (Fig. S3B). We did not observe any expression of immunoglobulins, nor did we observe expression of fibrinogen subunits (*FGA*, *FGB*, or *FGG* genes; Fig. S3C). A few of the proteins of interest were expressed in modest to high levels in some cell types (e.g., *MIA3*, *PPAB2B*), whereas *KNG1* was expressed across all the identified cell types. However, the majority of the proteins of interest were only expressed at very low levels or not at all (Fig. S3C). For example, it is well known that *FGA*, *FGB*, or *FGG* are almost exclusively synthesized by hepatocytes in the liver and secreted to the blood plasma [43]. This indicates that the presence of these proteins in the brain tissue is probably due to extravasation into the brain parenchyma.

Recognition of fibrinogen by immunoglobulins is enriched in MSA

Next, we turned our focus to fibrinogen since accumulation of fibrinogen in brain tissue has been proposed as an active contributing factor in the inflammatory response in various neurological disorders (reviewed by Petersen, Ryu [44]). We identified seven potential confounding factors to our fibrinogen measurements which we investigated further. We noticed a persistent increase in total fibrinogen intensities in MSA patients relative to CTRLs across all protein extraction batches, an increase that was significantly different in extraction batch 2 (Fig. S4A). We

did not observe any correlations between total fibrinogen intensities and the remaining putative confounders, i.e., sex, post-mortem interval (PMI), age at sampling, disease duration, sample protein concentration, MSA subtype (Bonferroni-adj. $p > 0.007$; Fig. S4B–G).

Then, we wished to investigate the possible association between the increased levels of both immunoglobulins and fibrinogen in brain tissue of MSA patients. Immunoglobulins and immunoglobulin–antigen complexes were isolated from groupwise pools of brain lysates using naked protein G-coupled beads and analyzed using LC–MS/MS (Fig. 2A). We identified 2,231 unique proteins across the groupwise pools. Among these, 115 proteins were immunoglobulins that were responsible for 31–98% of the total MS1 intensity (Fig. S5A). The immunoglobulin proteins were excluded from the downstream analyses along with proteins that were not identified in all groupwise pools. The resulting list contained 259 proteins including 16 proteins showing nominally significantly different abundances between groups (Table S12). Of the 49 proteins identified with differential expression in the brain extracts, *FGA*, *FGB*, *FGG*, and haptoglobin (HP) were captured in all pools. Furthermore, *FGB* and *FGG* were among the nominally significantly different proteins showing increased levels in the MSA pools compared with the CTRL pools (Mann–Whitney U test, $p = 0.05$; Fig. 2B). The specificity of the Ig–antigen coupling was confirmed by analyzing antigen binding to Protein G beads saturated with isotype control antibodies (Fig. S5B). Analysis of a blank sample showed some unspecific carry-over of HP, a high-abundant serum protein (Fig. S5B). Hence, the results indicate immunoglobulin recognition of fibrinogen subunits, which is enriched in MSA patients. Additionally, differences in protein intensities for other relevant target proteins, including αSyn , were interrogated, but did not show any differences between the groups (Fig. S5C).

Based on fibrinogen subunit intensities being increased in both single samples and groupwise pool samples, we sought to validate our MS data by analyzing a subset of the initial brain protein extracts by western blotting. A representative western blot is shown in Fig. 2C. We targeted *FGB* as a representative for fibrinogen and we confirmed increased levels of *FGB* in MSA brains compared with CTRLs (t test, $p = 0.015$; Fig. 2C; raw blots are shown in Fig. S6).

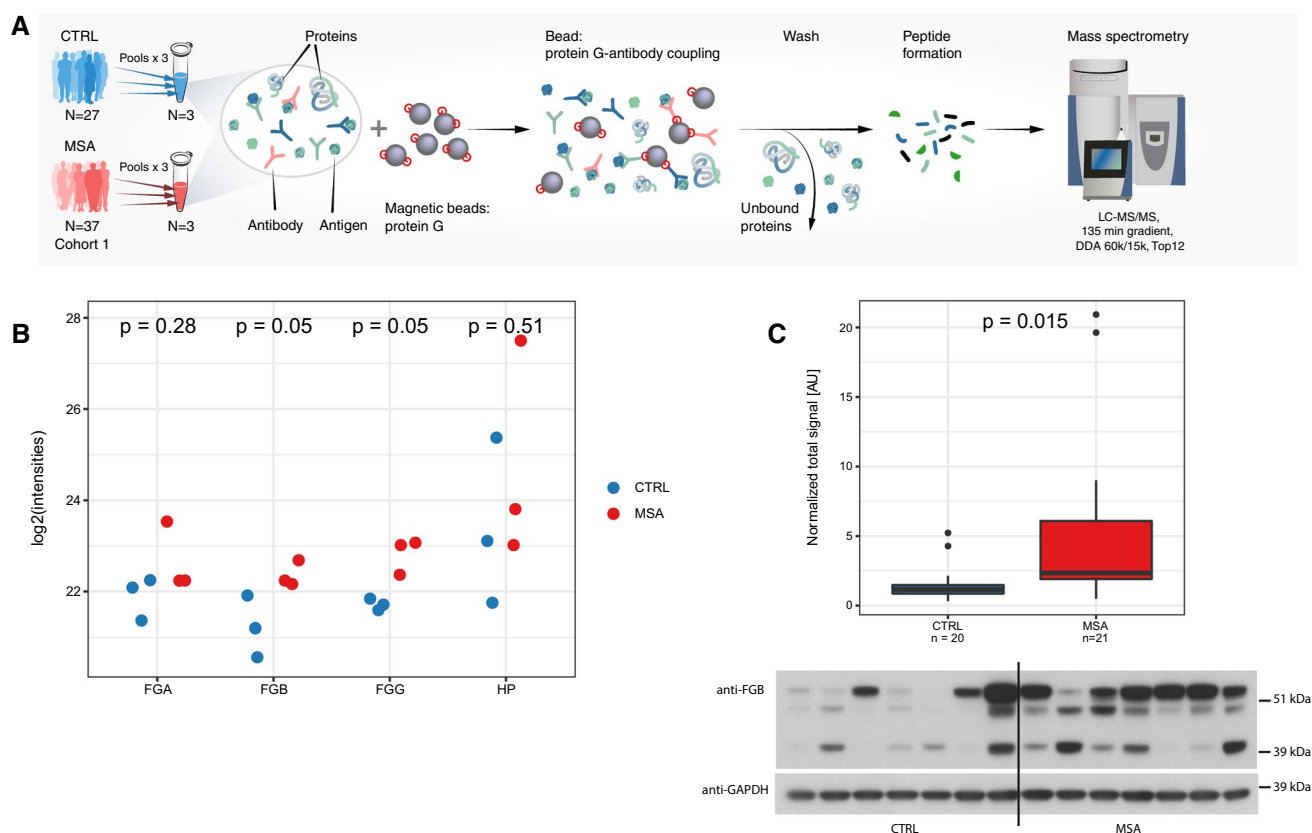


Fig. 2 The blood-clotting factor fibrinogen accumulates in multiple system atrophy brain tissue and is recognized by the immune system. **A** Experimental and data analysis workflow for validation experiment. From the brain sample cohort 1, groupwise sample pools were made in triplicates for immuno-capture using magnetic beads with Protein G for isolation of immunoglobulin:antigen complexes. Unbound proteins were removed by washing before peptide formation and analysis using mass spectrometry. **B** Intensity levels of target proteins that were immunocaptured and detected in all pools. Significance was assessed using a Mann–Whitney *U* test. There was increased immune recognition of fibrinogen beta (FGB) and gamma (FGG) in MSA brains. **C** Immunoblotting experiments for detection of FGB was performed on a randomly selected sub-cohort of cohort

1. Detection of FGB in brain extracts by western blotting probing with Rb-a-Hu FGB antibody. Three bands for FGB were recognized, two around 50 kDa in good agreement with the expected mass (56 kDa), and one band at 39 kDa possibly representing a truncated form of FGB. Intensities of all three bands were considered. GAPDH was used for normalization of the signal. Box plot showing immunoblot results for quantification of FGB protein levels, data are shown relative to the signal from normal, healthy controls (CTRL). Boxes show 1st (Q1) to 3rd (Q3) quartile of data, the horizontal line shows the median, and the whiskers show Q1 inter-quartile range (IQR; lower whisker) or Q3 + IQR (upper whisker). Outliers are shown with dots. Significance was assessed using a *t* test

Fibrinogen accumulates around blood vessels in MSA brains

We wanted to establish whether the increased levels of fibrinogen in MSA brains were due to extravasation from the blood stream. Thus, formalin-fixed MSA brain tissue blocks from the prefrontal cortex were lipid-cleared and stained for FGB and for glial fibrillary acidic protein (GFAP) as a marker for astrocytic end-feet supporting BBB integrity. After 3D reconstruction of images, FGB reactivity was observed in the brain parenchyma as perivascular smears. These smears were often of lower intensity compared to the intravascular fraction of fibrinogen (Fig. 3A).

GFAP was changed mostly regarding the astrocytic end-feet processes. In MSA, these end-feet processes were less well defined compared with controls. This could be the result of hypertrophic cell bodies, which were observed to some extent (Fig. 3B, video GFAP and FGB, Online Resource). Following these observations, we wanted to measure the area of fibrinogen deposition around blood vessels using an approach previously performed on brain tissue from Alzheimer's disease (AD) patients [45, 46]. Using brain slides from four MSA and four CTRL brains, we estimated the anti-FGB-immunoreactive areas surrounding randomly selected blood vessels using a stereological approach (Figures S7A–B; example shown in Fig. 3C). The number of blood vessels surrounded by FGB-immunoreactive areas did not differ between MSA and CTRL brains (Mann–Whitney

U test; $p=0.100$; Fig. S7C), nor was the fraction of FGB-immunoreactive area of the total area per slide different (Mann–Whitney U test; $p=0.490$; Fig. S7D). In contrast, in MSA patients, we observed a tendency toward larger FGB-immunoreactive areas around blood vessels (Mann–Whitney U test, $p=0.057$; Fig. 3D). These results indicate that the high fibrinogen levels found in MSA brains according to our MS data are likely due to an increased extravasation from the blood to the brain parenchyma in these patients. Further, we investigated by immunofluorescence on FFPE brain tissue slices from MSA patients and CTRLs how fibrinogen was deposited in the brain. We observed FGB immunoreactivity in different cells of the brain as well as co-localization of FGB with GFAP⁺ and NeuN⁺ cells of the brain in both sample groups (Figs. 3E, F, S7E–G).

BBB leakage markers are increased in plasma in MSA

The next step was to investigate if an increased BBB permeability in MSA patients could explain the increased fibrinogen extravasation found in MSA brains. For that purpose, we applied immunoblotting to assess blood plasma levels of two well-established BBB leakage protein markers, GFAP and neurofilament light chain (NFL), in a second cohort of 20 MSA patients and 20 CTRLs (cohort 2, Tables 1 and S3). For both markers, we observed elevated protein plasma levels of MSA patients compared with CTRLs indicating increased BBB permeability in the MSA patients (t test, $p<0.05$; Fig. 3G, H).

We assessed if GFAP or NFL protein levels correlated with either motor severity or disease duration. For GFAP, we found a moderate correlation with motor severity ($p=0.042$), whereas we saw a tendency for NFL ($p=0.067$; Fig. 3I). For disease duration, we found a moderate correlation for NFL ($p=0.035$) but none for GFAP ($p=0.64$; Fig. 3J). We did not observe any correlation to age at sampling, or any sex differences ($p>0.05$; Fig. S7H, I). These results further support that increased BBB permeability is a feature in MSA patients and that this is associated with disease progression.

Soluble fibrinogen is increased in the CSF from atypical Parkinsonism disease patients

We then wanted to investigate to what extent fibrinogen extravasation in the brain was reflected in the CSF. We aimed at clarifying both the translatability of our results from brain tissue to the CSF, as well as the potential for fibrinogen as a CSF prognostic biomarker for MSA. To determine the specificity of aberrant fibrinogen protein levels in the CSF, we included samples from related atypical parkinsonian disorders. Hence, we included CSF samples

from a cohort consisting of 28 MSA, 20 DLB, and 39 PSP patients, together representing atypical parkinsonism patients, along with samples from 40 PD patients and 17 CTRLs (cohort 3, Tables 1 and S4). The samples were separated into fractions containing micro-vesicles, exosomes and genuine soluble proteins by differential centrifugation, and each fraction was digested with trypsin and resulting peptide mixtures analyzed by LC–MS/MS using data-independent acquisition (DIA) with fast LC gradients (Fig. 4A).

Using this proteomics approach, we separated the CSF proteins depending on their biological compartmentalization. We were able to detect a total of 866–1168 CSF proteins in the fractions (Fig. S8A–C). We observed a very weak yet significant correlation between the time from sampling to freezing and the number of proteins in the exosomal fraction ($p=0.027$) but not in the micro-vesicular or the soluble fractions ($p>0.05$; Fig. S8D). Proteins exhibiting nominal, significantly different protein intensities between each disease group and CTRLs are shown in Tables S13–15. A principal component analysis showed good distinction between the different fractions underlining the relevance of our pre-analysis fractionation (Fig. 4B).

In the soluble fraction, the total fibrinogen intensities were significantly different between groups (ANOVA, $p=0.009$), and the intensities were significantly elevated in the MSA, DLB, and PSP patients compared with CTRLs (Dunnett's post hoc test, $p<0.05$; Fig. 4C) but not in the PD patients compared with CTRLs ($p>0.05$). Plots comparing fibrinogen subunit abundance levels are shown in Fig. S8E–G. Total fibrinogen intensities were not different between groups in the micro-vesicular or exosomal fractions (Figures S8H–I). Additionally, we did not observe any differences in fibrinogen subunit concentrations in the micro-vesicular or exosomal fractions (data not shown). We did not identify any significant correlations to the total fibrinogen intensities in the soluble fraction of the CSF (Bonferroni-adj. $p>0.01$; Fig. S9A–E).

Then, we performed receiver and operator characteristic (ROC) analyses of total fibrinogen levels for each disease group compared with CTRLs. We observed a moderate discrepancy for total fibrinogen intensities for MSA, DLB, and PSP patients compared with CTRLs (AUC=0.733, AUC=0.753, AUC=0.691, respectively, Fig. 4D). For PD patients, we observed a low discrepancy compared with CTRLs (AUC=0.568; Fig. 4D). Similar observations were made for single fibrinogen subunits (Fig. S10A–C).

Lastly, we performed pathway analyses on the nominally significant genes per disease group compared with CTRLs (Tables S13–15). We clustered the five most significant terms from the GO, Reactome, and PANTHER databases per disease group. In the soluble fraction, we observed clusters of terms that overlapped between MSA, DLB, and PSP patients, whereas significant terms for PD patients clustered

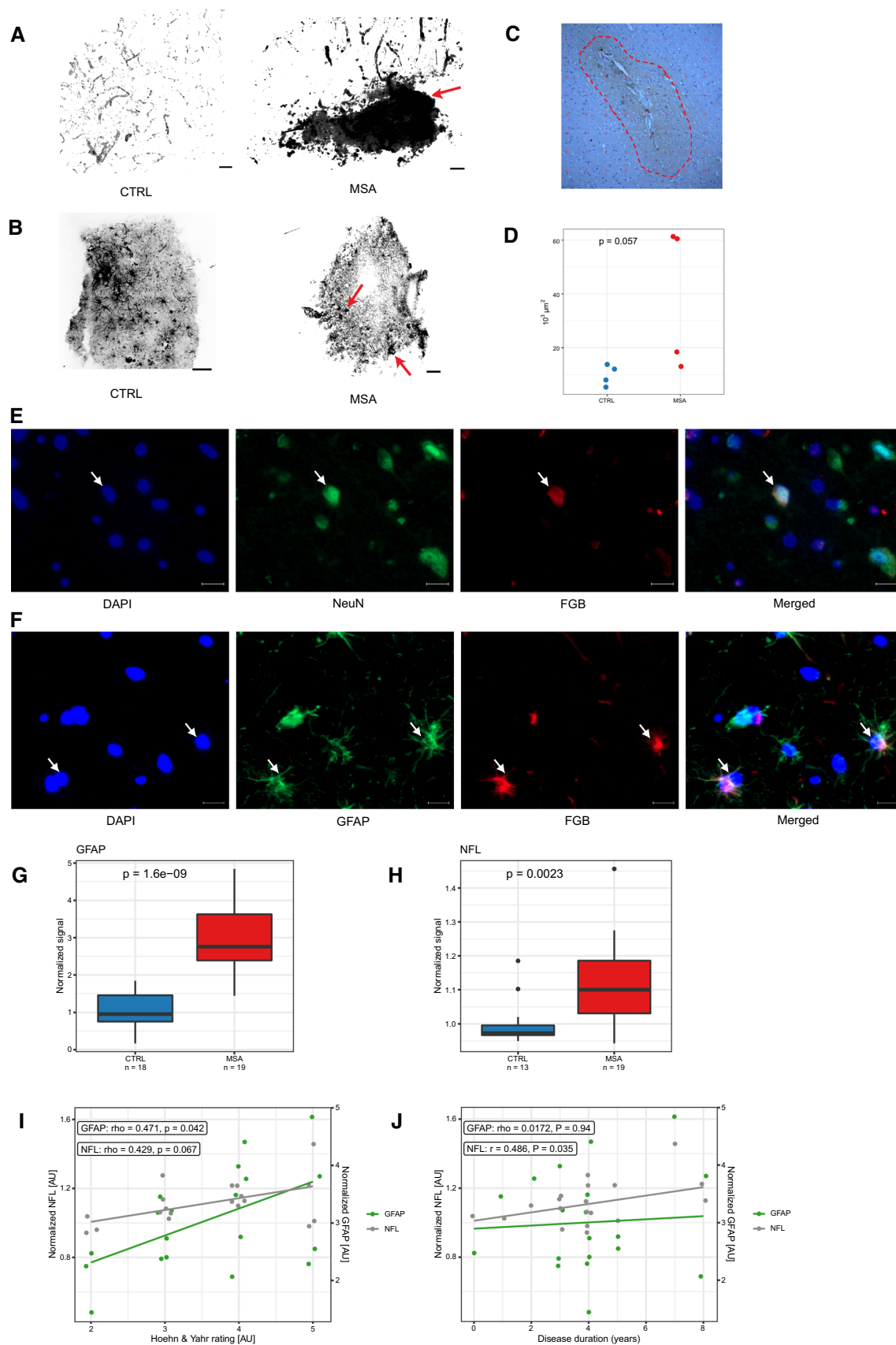


Fig. 3 Extravasation of fibrinogen around blood vessels in the MSA brain parenchyma, co-localization with astrocytes and neurons and blood–brain barrier leakage in MSA patients. **A, B** 3D reconstruction images acquired by a spinning disk confocal microscope for fibrinogen (FGB; **A**) or glial fibrillary acidic protein (GFAP; **B**). In **A**, FGB leakages are marked with an arrow, in **B** hypertrophic cell bodies are marked by an arrow. Scale bar=30 μ m. **C** Representative blood vessel from an MSA patient. The dotted outline shows faint brown immunoreactivity against FGB. The contrast was adjusted to highlight FGB deposition. A point grid was used for quantifying the area within the red dotted line in randomly selected blood vessel breaches in four MSA and four CTL brains. Scale bar=100 μ m. **D** Mean FGB⁺ immuno-reactive area per breach per sample. Significance assessed using a Mann–Whitney *U* test. **E, F** Double immunofluorescence labeling showing co-localization (arrows) of FGB in **E** neurons (NeuN⁺ cells) or **F** astrocytes (GFAP⁺ cells) in MSA brain tissue samples. Scale bar=20 μ m. **G–H** Box plots for BBB leakage markers glial fibrillary acidic protein (GFAP; **G**) or neuro-filament light chain (NFL; **H**) measured in plasma samples from 20 CTRLs and 20 MSA patients. Significance was assessed using a *t* test. Only samples with quantifiable levels of a target protein are shown. Boxes show 1st (Q1) to 3rd (Q3) quartile of data, the horizontal line shows the median, and the whiskers show Q1 inter-quartile range (IQR; lower whisker) or Q3+IQR (upper whisker). Points represent putative outliers which are included still in the analysis. **I** Plasma GFAP or NFL protein levels plotted against the Hoehn & Yahr rating. Significant correlations were assessed using Spearman's rank correlation test. **J** Plasma levels of GFAP or NFL plotted against the disease duration. For GFAP, Spearman's rank correlation test was used. For NFL, the Pearson's product-moment correlation test was used. CTRL: normal, healthy controls

distinct to the terms from the atypical parkinsonian patients (Fig. 4E). In the micro-vesicle fraction, we observed some clusters containing overlapping terms between atypical parkinsonian patients (Fig. S10D), whereas no overlap was observed for the exosomal fraction (Fig. S10E).

Discussion

In the present study, we investigated the proteome in the prefrontal cortex of 45 MSA patients and 30 CTRLs. We applied an unbiased, global, MS-based proteomics approach, which allowed for quantification of 4348 proteins. We identified overrepresentation of components of the coagulation as well as the complement cascade in MSA patients. Blood clotting components included fibrinogen subunits FGA, FGB, and FGG, as well as PLG and F2 among other. To our knowledge, this is the first time to describe involvement of the coagulation cascade and fibrinogen accumulation in brain tissue from MSA patients. By immuno-capture, we showed that immunoglobulin recognition of fibrinogen is enriched in MSA patients. Furthermore, we observed fibrinogen deposition in the brain parenchyma surrounding blood vessels which is likely indicative of BBB aperture. This increase in BBB leakage was already present during the disease course in MSA patients and correlated with disease

progression as demonstrated by use of plasma samples. Lastly, we showed that elevated levels of fibrinogen were detectable in the CSF, not only in MSA patients but also in the other atypical parkinsonian disorders DLB and PSP, while fibrinogen intensity was unchanged in the CSF of PD patients.

Fibrinogen is a plasma protein synthesized in the liver and is essential for wound healing leading to fibrin deposition and activation of platelets to form blood clots (reviewed by Fish and Neerman-Arbez [43]). Accumulation of fibrinogen in brain tissue has been previously associated with neurodegeneration in other brain disorders, including multiple sclerosis [47] and AD [46]. In AD brains, fibrinogen interacts with β -amyloid [48] altering fibrinolysis and thrombosis, thereby possibly contributing to plaque formation [49]. In our study, we observed accumulation of fibrinogen around blood vessels, suggesting impaired fibrinolysis in MSA brains too. F2, necessary for fibrinogen cleavage into fibrin, was similarly increased in the MSA brains indicating increased fibrin fiber production. Fibrin co-localizes with surface receptors in microglia, neurons, and astrocytes, and activates cell intrinsic pathways involved in immune responses [8]. Neuro-inflammation and activation of the coagulation cascade are intrinsically co-regulated [50], as F2, PLG and kallikrein are activators of the complement cascade. These components are among the up-regulated proteins in MSA brains similar to CFB, initiator of the alternative complement pathway [51]. Together, these observations support our belief of a strong neuro-inflammatory condition in MSA brains that likely involve coagulation and fibrinolysis processes at the neurovascular interface.

Pathologically, brain accumulation of fibrinogen or its active coagulation component fibrin, has been linked to demyelination and autoimmunity accompanied with increased antigen presentation in cells of the brain [52], possibly enhanced by PLG-dependent fibrinolysis [53]. The contribution of fibrinogen to immune reactivity in neurodegeneration was further substantiated in a magnetic resonance imaging study showing a spatiotemporal relationship of fibrinogen leakage and immune responses in a model of experimental autoimmune encephalomyelitis [54]. Of relevance, it has been shown that accumulation of fibrinogen in brain tissue leads to activation of microglia in an AD model [55]. Additionally, rat primary microglia stimulated with fibrin are enriched for processes for antigen presentation [52]. This relates well to our previous observations of increased microglial numbers [1] and increased Toll-like receptor gene expression (10) in brains of MSA patients. The increased brain fibrinogen accumulation reported in this study is likely reflecting an activated neuro-inflammatory condition in MSA brains. Previously, we have shown increased micro- and astrogliosis, and cytokine protein levels, specifically interleukin 2 (IL-2), in MSA patients in the

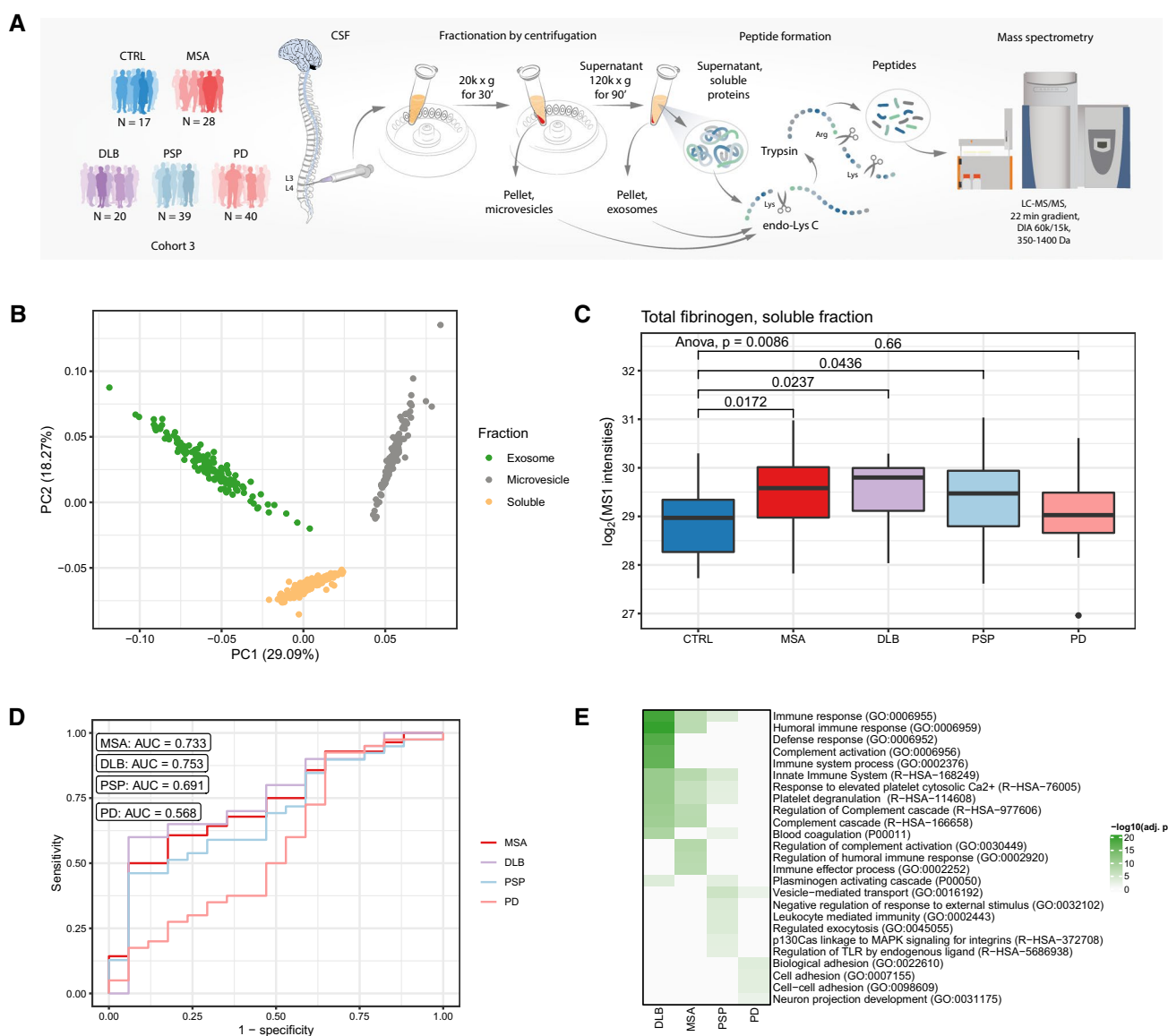


Fig. 4 Fibrinogen protein levels are elevated in the cerebrospinal fluid (CSF) of atypical parkinsonian patients. **A** Experimental workflow showing cerebrospinal fluid sample fractionation and analysis. CSF samples were fractionated by repeated centrifugation before tryptic digestion prior to analysis by mass spectrometry. **B** Principal component analysis of CSF samples from all fractions. **C** Box plots showing total fibrinogen protein intensities in the soluble fraction of the CSF. Boxes show 1st (Q1) to 3rd (Q3) quartile of data, the horizontal line shows the median, and the whiskers show Q1 inter-quartile range (IQR; lower whisker) or Q3 + IQR (upper whisker). Outliers

are shown with dots. Significance was assessed using an ANOVA test followed by Dunnett's post hoc test for multiple comparisons against the normal, healthy controls (CTRLs). **D** Line plots showing results from receiver and operator characteristic analyses on total fibrinogen from the soluble proteins fraction of each disease group versus CTRLs. **E** Heatmap of pathway analyses clustered by similarity. MSA multiple system atrophy, DLB dementia with Lewy bodies, PSP progressive supra-nuclear palsy, PD Parkinson's disease, AUC area under the curve

same brain area as the one investigated here [1, 9]. IL-2 is a pro-inflammatory cytokine induced by antigen activation that regulates T cell and natural killer cell responses (reviewed by Rydbirk, Elfving [56]). Increased IL-2 can be pathogenic and is believed to drive capillary leak syndrome associated with excessive complement activation, endothelial injury, and dysregulation in the coagulation cascade as

seen in cytokine storms for COVID-19 infections [57]. The fact that we see in this study both an overrepresentation of the coagulation and complement cascade and an increased BBB permeability in MSA patients, together with the previous finding of increased IL-2 levels [5], may suggest a hyper-activation of the immune system in MSA brains. There are reports of α Syn driving T cell responses in PD

patients [58] even at prodromal stages [59] pointing to an autoimmune response in these types of diseases. In support of this, in MSA patients, we have previously shown an aberrant autoantibody recognition of α Syn when compared to CTRLs in blood [60, 61] and in CSF samples [62], besides an increase of global immunoglobulin IgG1 (the major IgG subclass of IgGs) in CSF [62].

BBB dysfunction has been linked to the development of several neurodegenerative diseases, including PD, AD, and multiple sclerosis [44, 46, 47, 54, 55]. Furthermore, macrophages of the immune system have been proposed as a contributing factor to BBB damage in AD [45]. During sustained inflammation, microglia attacks astrocytic end-feet, which impairs BBB function [63] and possibly increasing BBB permeability. In the present study, our results on cleared tissue supported the finding that fibrinogen entered the brain parenchyma, which is indicative of BBB dysfunction and increased permeability. Some smearing of the intravascular component could potentially take place during preparation of tissue blocks by cutting, but in optically cleared specimens, this cannot take place. Further supporting these results, we identified increased levels of different extracellular matrix proteins in our MS data, which may indicate a weakened BBB basal membrane in MSA patients since the composition of extracellular matrix proteins is altered upon BBB disruption [64]. Also, previous studies have shown a correlation between BBB leakage and disease progression in MSA using both a CSF albumin index and MRI [65]. BBB leakage can be reflected in the blood by the increased presence of proteins largely specific to the brain, and therefore have long been proposed as potential biomarkers of both cerebral tissue damage and BBB leakage [66]. NFL and GFAP are key structural proteins associated with neurons and astroglia, respectively. These proteins have shown promise as potential tools for differentiation between healthy aging and cognitive decline [67] as well as among dementia patients [68]. In the present study, we showed elevated levels of both NFL and GFAP protein levels in plasma from MSA patients compared with CTRLs. In MSA, NFL has been shown repeatedly to be increased in blood [69–71] or CSF [72] compared with CTRLs and/or PD patients. Furthermore, blood and CSF NFL protein levels have been shown to correlate well [71, 73] showing a relatedness between leakage to different compartments of the body. To our knowledge, this is the first time a significant correlation between GFAP plasma protein levels and motor severity in MSA, assessed by the patients' Hoehn & Yahr rating, is being demonstrated. This suggests a relationship between BBB permeability and impaired motor skills. Similarly, in MSA we show for the first time a relationship between NFL plasma protein levels and patient disease duration. Blood NFL levels were previously shown to correlate with Hoehn & Yahr ratings [71] in a cohort spanning several

atypical parkinsonian disorders, including MSA suggesting that the tendency we report here might be supported in a larger cohort. Future studies on NFL plasma protein levels and MSA motor severity are warranted. In PD patients, correlations between elevated blood or CSF NFL protein levels and motor severity and/or disease duration have been previously shown [70, 71, 73]. Taken together, this cross-sectional study on plasma samples from MSA patients suggests that BBB leakage is present and is associated with disease worsening.

Whether fibrinogen interacts physically with α Syn and thereby contributing to pathological events could not be assessed in the present study. An interaction between fibrinogen and α Syn from hand ligament has been described [74]; however, to our knowledge, this observation has not been replicated in other experimental setups or on α Syn from brain tissue. Since fibrinogen contains several interaction hotspots for binding to other proteins (e.g., reviewed by Petersen, Ryu [44]), an interaction with α Syn is possible and relevant to investigate in studies more adequately designed for addressing this. Probably for the same reason, we failed to observe an enriched recognition of brain α Syn by immunoglobulins in our setup. This could be expected based on previous studies on blood or CSF immunity toward α Syn in MSA patients [60, 61]. Whether immune recognition of α Syn is mainly a peripheral phenomenon remains an open question.

The single-cell RNA sequencing data not only supported our hypothesis that the high presence of immunoglobulin and fibrinogen proteins is due to extravasation from the periphery to the brain parenchyma, but we also identified cell-specific expression of some protein-coding genes in the MSA brains, e.g., *PPAP2B*, *MIA3*, *KNG1*, *HSD17B11*. Specifically, *PPAP2B*, a phospholipid phosphatase that was down-regulated in MSA, is mainly expressed in astrocytes and oligodendrocyte precursor cells. *PPAP2B* protein deficiency leads to enhanced vascular inflammation and permeability [75]. Another interesting target is *MIA3*, also known as *TANGO1*, which is involved in enabling endoplasmic reticulum-to-Golgi trafficking of large proteins [76]. We found *MIA3* protein up-regulated in MSA, and we saw *MIA3* to be highly expressed in both excitatory and inhibitory neurons. However, in the present study, even though they may be interesting, we chose not to investigate further the role of these proteins in MSA pathology, nor did we investigate their possible contribution to MSA disease processes.

Finally, a third patient cohort determined that aberrant protein levels observed in brain tissue in our post-mortem study was reflected in the CSF profile of living MSA patients. The pre-analysis sample fragmentation that we perform here allows for a deep proteome coverage of the CSF samples. To our knowledge, no study has fractionated the samples prior to analysis similar to our approach, which

makes our results novel and not directly comparable to previous studies. Intensive efforts have been made to identify disease-specific biomarkers for MSA. Our results point toward increased fibrinogen levels in the CSF as a potential biomarker, not only for MSA but in general for atypical parkinsonian diseases. Further studies should investigate the diagnostic validity of these findings. In PD, several candidates have been evaluated, and some have even been validated in different studies (reviewed by Halbgebauer, Öckl [77]). In the CSF, this includes FGB, HP, APOA1, APOA2, and GC proteins which we show are up-regulated in brain tissue of MSA patients. However, results from studies on CSF samples are seemingly divergent with some studies showing up-regulated protein levels of these targets whereas other find down-regulated protein levels [77]. Similarly, several blood studies in PD also report differential levels of some of the target proteins that we identified (APOA1, APOA2, HP), but contrary to the upregulation observed by us in the brain, they found reduced blood protein levels [77]. Most important, the CSF results indicate that the fibrinogen accumulation observed in MSA brains is not only present at end-stage disease phases. Furthermore, fibrinogen accumulation could be a mechanism present during the disease course specific for atypical parkinsonian disorders, which are diseases with a much more severe disease profile than other better-described neurodegenerative diseases such as PD.

Our current study holds some limitations. Protein activity is often regulated by post-translational modifications (PTMs) such as site-specific phosphorylation, but due to the sub-stoichiometric nature of PTMs, specific enrichment prior to MS analysis is required (reviewed by Thygesen, Boll [78]). In the present setup, the primary aim was not to investigate PTMs but this may, however, prove relevant for the aberrantly expressed proteins identified here. Further, it would be interesting to investigate whether the aberrant levels of several proteins we observe in the frontal cortex are mirrored in other brain regions as well. In regards of the single-cell RNA sequencing data, although we acquired data from the frontal cortex, these data were not prepared for the same area that we investigated. Therefore, it is possible that we would have identified additional cell types expressing our proteins of interest if we had had data for the exact area that we used for discovery proteomics. Based on the latest development in single-cell MS [79], it would be relevant to investigate levels of significant proteins in single cells to verify cell types contributing to the changes in MSA described here. Even though our CSF sample cohort was substantial, distinguishing MSA patients from CTRLs in CSF samples through total fibrinogen measurements were not exceptionally good as assessed by AUC measurements. Power calculations showed that to obtain a type II error rate of 5%, we would need to at least double the number of CTRL samples in our setup. Therefore, we wish to address this in future

studies with larger sample cohorts, especially with higher CTRL samples. Also, including analysis of CSF D-dimer levels could give us a more direct indication of whether fibrinolysis is altered in these patients.

Conclusion

To conclude, in the prefrontal cortex of MSA patients, we identified increased levels of immune system components and blood-clotting factors, with fibrinogen protein levels being one of the highest. Brain fibrinogen accumulation was accompanied by enhanced immune system recognition in MSA patients. We observed increased fibrinogen protein accumulation in the brain parenchyma surrounding blood vessels in MSA patients, and this was associated with increased BBB permeability. BBB permeability was correlated to disease severity and duration. Finally, we demonstrated that the increased brain fibrinogen protein levels were reflected in the soluble fraction of the CSF, something that was observed across atypical parkinsonian disorders. These results further support that pro-inflammatory responses are important contributors to the pathogenesis behind MSA.

Supplementary Information The online version contains supplementary material available at <https://doi.org/10.1007/s00018-022-04378-z>.

Acknowledgements The MRC London Brain Bank for Neurodegenerative Diseases provided some of the samples for the present study. The authors are grateful to Hans Jørgen Jensen and Susanne Sørensen for help with conducting experiments.

Authors' contributions Study concept and design: RR, OØ, SA, JVO, BP, TB, JF. Collection of brain samples: BP, TB. Collection of plasma samples: AL, AMH, MB, MB, MM, EHD. Collection of CSF samples: LS, CCS, SB, KW. Acquisition of experimental data: OØ, RR, CH, BDV. Securing infrastructure: JVO, BP, SA, JR, TLA. Analysis and interpretation of data: OØ, RR, SA, JVO. Wrote the manuscript: RR, OØ, SA. All authors read and approved the final manuscript.

Funding This work has been supported by the Brdr. Hartmann Foundation, Oda og Hans Svenningsens Fond, the Hørslev Foundation, the Jascha Foundation, Danmodis, the Parkinson Foundation Denmark, the Lundbeck Foundation, the Research Foundation of Bispebjerg-Frederiksberg Hospital, the Danish National Association for Multiple System Atrophy and the Novo Nordisk Foundation (grant no. NNF14CC0001). The sponsors were not involved in the design of the study, data collection, analysis, or interpretation, preparation of the manuscript, or in the decision to publish.

Availability of data and materials The LC-MS/MS datasets supporting the conclusions of this article are available through ProteomeXchange with the identifiers PXD026370 (brain samples) or PXD026802 (CSF samples).

Declarations

Conflict of interest The authors declare no conflict of interest and have not received any funding, or benefits from industry or for-profit organization for this work. BDV is an employee of GLX Analytix ApS. He declares no financial interest.

Ethics approval and consent to participate This project was approved by the regional ethical committee of the Capitol Region (Denmark), j.nr. H-16025210 and H-15016232 and the Danish data protection agency (j.nr. P-2020-937). All Danish donors provided informed written consent, whereas informed, written consent was provided either by British donors or their next of kin.

Consent for publication Not applicable

References


- Salvesen L, Winge K, Brudek T, Agander TK, Løkkegaard A, Pakkenberg B (2017) Neocortical neuronal loss in patients with multiple system atrophy: a stereological study. *Cereb Cortex* 27(1):400–410
- Monzio Compagnoni G, Di Fonzo A (2019) Understanding the pathogenesis of multiple system atrophy: state of the art and future perspectives. *Acta Neuropathol Commun* 7(1):113
- Iba M, Kim C, Sallin M, Kwon S, Verma A, Overk C et al (2020) Neuroinflammation is associated with infiltration of T cells in Lewy body disease and α -synuclein transgenic models. *J Neuroinflammation* 17(1):214
- Williams GP, Marmion DJ, Schonhoff AM, Jurkuvenaite A, Won W-J, Standaert DG et al (2020) T cell infiltration in both human multiple system atrophy and a novel mouse model of the disease. *Acta Neuropathol* 139(5):855–874
- Pediaditakis I, Kodella KR, Manatakis DV, Le CY, Hinojosa CD, Tien-Street W et al (2021) Modeling alpha-synuclein pathology in a human brain-chip to assess blood-brain barrier disruption. *Nat Commun* 12(1):5907
- Elabi O, Gaceb A, Carlsson R, Padel T, Soylu-Kucharz R, Cortijo I et al (2021) Human α -synuclein overexpression in a mouse model of Parkinson's disease leads to vascular pathology, blood brain barrier leakage and pericyte activation. *Sci Rep* 11(1):1120
- Schaeffer S, Iadecola C (2021) Revisiting the neurovascular unit. *Nat Neurosci* 24(9):1198–1209
- Bardehle S, Rafalski VA, Akassoglou K (2015) Breaking boundaries-coagulation and fibrinolysis at the neurovascular interface. *Front Cell Neurosci* 9:354
- Rydbirk R, Elfving B, Andersen MD, Langbøl MA, Folke J, Winge K et al (2017) Cytokine profiling in the prefrontal cortex of Parkinson's Disease and Multiple System Atrophy patients. *Neurobiol Dis* 106:269–278
- Brudek T, Winge K, Agander TK, Pakkenberg B (2013) Screening of Toll-like receptors expression in multiple system atrophy brains. *Neurochem Res* 38(6):1252–1259
- Rydbirk R, Folke J, Busato F, Roché E, Chauhan AS, Løkkegaard A et al (2020) Epigenetic modulation of ARL1 and increased HLA expression in brains of multiple system atrophy patients. *Acta Neuropathol Commun* 8(1):29
- World Medical Association Declaration of Helsinki (2013) ethical principles for medical research involving human subjects. *JAMA* 310(20):2191–2194
- Bradford MM (1976) A rapid and sensitive method for the quantitation of microgram quantities of protein utilizing the principle of protein-dye binding. *Anal Biochem* 72:248–254
- Kelstrup CD, Bekker-Jensen DB, Arrey TN, Hogrebe A, Harder A, Olsen JV (2018) Performance evaluation of the Q exactive HF-X for shotgun proteomics. *J Proteome Res* 17(1):727–738
- Hoehn MM, Yahr MD (1967) Parkinsonism. Onset, progression, and mortality. 17(5):427–42
- DellaValle B, Hasseldam H, Johansen FF, Iversen HK, Rungby J, Hempel C (2019) Multiple soluble components of the glycocalyx are increased in patient plasma after ischemic stroke. *Stroke* 50(10):2948–2951
- Schneider CA, Rasband WS, Eliceiri KW (2012) NIH Image to ImageJ: 25 years of image analysis. *Nat Methods* 9(7):671–675
- Messal HA, Almagro J, Zaw Thin M, Tedeschi A, Ciccarelli A, Blackie L et al (2021) Antigen retrieval and clearing for whole-organ immunofluorescence by FLASH. *Nat Protoc* 16(1):239–262
- Klingberg A, Hasenberg A, Ludwig-Portugall I, Medyukhina A, Männ L, Brenzel A et al (2017) Fully automated evaluation of total glomerular number and capillary tuft size in nephritic kidneys using lightsheet microscopy. *J Am Soc Nephrol* 28(2):452–459
- Rueden CT, Schindelin J, Hiner MC, DeZonia BE, Walter AE, Arena ET et al (2017) ImageJ2: ImageJ for the next generation of scientific image data. *BMC Bioinform* 18(1):529
- Napari contributors (2019) napari: a multi-dimensional image viewer for python. 10.5281/zenodo.3555620
- Rappsilber J, Mann M, Ishihama Y (2007) Protocol for micro-purification, enrichment, pre-fractionation and storage of peptides for proteomics using StageTips. *Nat Protoc* 2(8):1896–1906
- Bekker-Jensen DB, Martínez-Val A, Steigerwald S, Rütger P, Fort KL, Arrey TN et al (2020) A compact quadrupole-Orbitrap mass spectrometer with faims interface improves proteome coverage in short lc gradients. *Mol Cell Proteomics* 19(4):716–729
- Cox J, Mann M (2008) MaxQuant enables high peptide identification rates, individualized p.p.b.-range mass accuracies and proteome-wide protein quantification. *Nat Biotechnol* 26(12):1367–1372
- Cox J, Neuhauser N, Michalski A, Scheltema RA, Olsen JV, Mann M (2011) Andromeda: a peptide search engine integrated into the MaxQuant environment. *J Proteome Res* 10(4):1794–1805
- Schwanhäusser B, Busse D, Li N, Dittmar G, Schuchhardt J, Wolf J et al (2011) Global quantification of mammalian gene expression control. *Nature* 473(7347):337–342
- Perez-Riverol Y, Csordas A, Bai J, Bernal-Llinares M, Hewapathirana S, Kundu DJ et al (2019) The PRIDE database and related tools and resources in 2019: improving support for quantification data. *Nucleic Acids Res* 47(D1):D442–D450
- Bruderer R, Bernhardt OM, Gandhi T, Miladinović SM, Cheng LY, Messner S et al (2015) Extending the limits of quantitative proteome profiling with data-independent acquisition and application to acetaminophen-treated three-dimensional liver microtissues. *Mol Cell Proteom* 14(5):1400–1410
- Koopmans F, van Nierop P, Andres-Alonso M, Byrnes A, Cijssouw T, Coba MP et al (2019) SynGO: an evidence-based, expert-curated knowledge base for the synapse. *Neuron* 103(2):217–34. e4
- Kuhn M. Building Predictive Models in R Using the caret Package. 2008;28(5):1-26
- R Core Team. R: A Language and Environment for Statistical Computing (2021) R foundation for statistical computing. Austria, Vienna
- Barkas N, Petukhov V, Kharchenko P, Biederstedt E (2021) pagoda2: single cell analysis and differential expression. R package version 102

33. Barkas N, Petukhov V, Nikolaeva D, Lozinsky Y, Demharter S, Khodosevich K et al (2019) Joint analysis of heterogeneous single-cell RNA-seq dataset collections. *Nat Methods* 16(8):695–698
34. Fabregat A, Jupe S, Matthews L, Sidiropoulos K, Gillespie M, Garapati P et al (2018) The Reactome pathway knowledgebase. *Nucleic Acids Res* 46(D1):D649–D655
35. Thomas PD, Campbell MJ, Kejariwal A, Mi H, Karlak B, Daverman R et al (2003) PANTHER: a library of protein families and subfamilies indexed by function. *Genome Res* 13(9):2129–2141
36. Resource TGO (2019) 20 years and still GOing strong. *Nucleic Acids Res* 47(D1):D330–D338
37. Ashburner M, Ball CA, Blake JA, Botstein D, Butler H, Cherry JM et al (2000) Gene ontology: tool for the unification of biology. *Gene Ontol Consortium Nat Genet* 25(1):25–29
38. Szklarczyk D, Morris JH, Cook H, Kuhn M, Wyder S, Simonovic M et al (2017) The STRING database in 2017: quality-controlled protein-protein association networks, made broadly accessible. *Nucleic Acids Res* 45(D1):D362–D368
39. Legeay M, Doncheva NT, Morris JH, Jensen LJ (2020) Visualize omics data on networks with Omics Visualizer, a Cytoscape App. *F1000Res* 9:157. <https://doi.org/10.12688/f1000research.22280.2> (eCollection 2020)
40. Benjamini Y, Hochberg Y (1995) Controlling the false discovery rate: a practical and powerful approach to multiple testing. *J R Stat Soc* 57(1):289–300
41. Wickham H (2016) ggplot2: elegant graphics for data analysis. Springer
42. McHugh ML (2012) Interrater reliability: the kappa statistic. *Biochem Med (Zagreb)* 22(3):276–282
43. Fish RJ, Neerman-Arbez M (2012) Fibrinogen gene regulation. *Thromb Haemost* 108(3):419–426
44. Petersen MA, Ryu JK, Akassoglou K (2018) Fibrinogen in neurological diseases: mechanisms, imaging and therapeutics. *Nat Rev Neurosci* 19(5):283–301
45. Fiala M, Liu QN, Sayre J, Pop V, Brahmandam V, Graves MC et al (2002) Cyclooxygenase-2-positive macrophages infiltrate the Alzheimer's disease brain and damage the blood-brain barrier. *Eur J Clin Invest* 32(5):360–371
46. Ryu JK, McLarnon JG (2009) A leaky blood-brain barrier, fibrinogen infiltration and microglial reactivity in inflamed Alzheimer's disease brain. *J Cell Mol Med* 13(9a):2911–2925
47. Vos CM, Geurts JJ, Montagne L, van Haastert ES, Bö L, van der Valk P et al (2005) Blood-brain barrier alterations in both focal and diffuse abnormalities on postmortem MRI in multiple sclerosis. *Neurobiol Dis* 20(3):953–960
48. Ahn HJ, Zamolodchikov D, Cortes-Canteli M, Norris EH, Glickman JF, Strickland S (2010) Alzheimer's disease peptide beta-amyloid interacts with fibrinogen and induces its oligomerization. *Proc Natl Acad Sci U S A* 107(50):21812–21817
49. Cortes-Canteli M, Paul J, Norris EH, Bronstein R, Ahn HJ, Zamolodchikov D et al (2010) Fibrinogen and beta-amyloid association alters thrombosis and fibrinolysis: a possible contributing factor to Alzheimer's disease. *Neuron* 66(5):695–709
50. Sun Y, Langer HF (2022) Platelets, thromboinflammation and neurovascular disease. *Front Immunol* 13:843404
51. Orsini F, De Blasio D, Zangari R, Zanier ER, De Simoni MG (2014) Versatility of the complement system in neuroinflammation, neurodegeneration and brain homeostasis. *Front Cell Neurosci* 8:380
52. Ryu JK, Petersen MA, Murray SG, Baeten KM, Meyer-Franke A, Chan JP et al (2015) Blood coagulation protein fibrinogen promotes autoimmunity and demyelination via chemokine release and antigen presentation. *Nat Commun* 6:8164
53. Shaw MA, Gao Z, McElhinney KE, Thornton S, Flick MJ, Lane A et al (2017) Plasminogen deficiency delays the onset and protects from demyelination and paralysis in autoimmune neuroinflammatory disease. *J Neurosci* 37(14):3776–3788
54. Lee NJ, Ha SK, Sati P, Absinta M, Luciano NJ, Lefeuve JA et al (2018) Spatiotemporal distribution of fibrinogen in marmoset and human inflammatory demyelination. *Brain* 141(6):1637–1649
55. Merlini M, Rafalski VA, Rios Coronado PE, Gill TM, Ellisman M, Muthukumar G et al (2019) Fibrinogen induces microglia-mediated spine elimination and cognitive impairment in an Alzheimer's disease model. *Neuron* 101(6):1099–108.e6
56. Rydbirk R, Elfving B, Folke J, Pakkenberg B, Winge K, Brudek T et al (2019) Increased prefrontal cortex interleukin-2 protein levels and shift in the peripheral T cell population in progressive supranuclear palsy patients. *Sci Rep* 9(1):7781
57. Mangalmurti N, Hunter CA (2020) Cytokine Storms: Understanding COVID-19. *Immunity* 53(1):19–25
58. Sulzer D, Alcalay RN, Garretti F, Cote L, Kanter E, Agin-Lieb J et al (2017) T cells from patients with Parkinson's disease recognize α -synuclein peptides. *Nature* 546(7660):656–661
59. Lindestam Arlehamn CS, Dhanwani R, Pham J, Kuan R, Frazier A, Rezende Dutra J et al (2020) α -Synuclein-specific T cell reactivity is associated with preclinical and early Parkinson's disease. *Nat Commun* 11(1):1875
60. Brudek T, Winge K, Rasmussen NB, Bahl JM, Tanassi J, Agander TK et al (2016) Altered α -synuclein, parkin, and synphilin isoform levels in multiple system atrophy brains. *J Neurochem* 136(1):172–185
61. Folke J, Rydbirk R, Løkkegaard A, Salvesen L, Hejl AM, Starhof C et al (2019) Distinct autoimmune anti- α -synuclein antibody patterns in multiple system atrophy and Parkinson's disease. *Front Immunol* 10:2253
62. Folke J, Rydbirk R, Løkkegaard A, Hejl A-M, Winge K, Starhof C et al (2021) Cerebrospinal fluid and plasma distribution of anti- α -synuclein IgMs and IgGs in multiple system atrophy and Parkinson's disease. *Parkinsonism Relat Disord* 87:98–104
63. Haruwaka K, Ikegami A, Tachibana Y, Ohno N, Konishi H, Hashimoto A et al (2019) Dual microglia effects on blood brain barrier permeability induced by systemic inflammation. *Nat Commun* 10(1):5816
64. Baeten KM, Akassoglou K (2011) Extracellular matrix and matrix receptors in blood-brain barrier formation and stroke. *Dev Neurobiol* 71(11):1018–1039
65. Song SK, Lee SK, Lee JJ, Lee JE, Choi HS, Sohn YH et al (2011) Blood-brain barrier impairment is functionally correlated with clinical severity in patients of multiple system atrophy. *Neurobiol Aging* 32(12):2183–2189
66. Janigro D, Bailey DM, Lehmann S, Badaut J, O'Flynn R, Hirtz C et al (2021) Peripheral blood and salivary biomarkers of blood-brain barrier permeability and neuronal damage: clinical and applied concepts. *Front Neurol*. <https://doi.org/10.3389/fneur.2020.577312>
67. Verberk IMW, Laarhuis MB, van den Bosch KA, Ebenau JL, van Leeuwenstijn M, Prins ND et al (2021) Serum markers glial fibrillary acidic protein and neurofilament light for prognosis and monitoring in cognitively normal older people: a prospective memory clinic-based cohort study. *The Lancet Healthy Longev* 2:e87–e95. [https://doi.org/10.1016/S2666-7568\(20\)30061-1](https://doi.org/10.1016/S2666-7568(20)30061-1)
68. Marques TM, van Rumund A, Oeckl P, Kuiperij HB, Esselink RAJ, Bloem BR et al (2019) Serum NFL discriminates Parkinson disease from atypical parkinsonisms. *Neurology* 92(13):e1479–e1486
69. Wilke C, Bender F, Hayer SN, Brockmann K, Schöls L, Kuhle J et al (2018) Serum neurofilament light is increased in multiple system atrophy of cerebellar type and in repeat-expansion spinocerebellar ataxias: a pilot study. *J Neurol* 265(7):1618–1624

70. Lin CH, Li CH, Yang KC, Lin FJ, Wu CC, Chieh JJ et al (2019) Blood NfL: a biomarker for disease severity and progression in Parkinson disease. *Neurology* 93(11):e1104–e1111
71. Hansson O, Janelidze S, Hall S, Magdalino N, Lees AJ, Andreasson U et al (2017) Blood-based NfL: a biomarker for differential diagnosis of parkinsonian disorder. *Neurology* 88(10):930–937
72. Holmberg B, Rosengren L, Karlsson J-E, Johnels B (1998) Increased cerebrospinal fluid levels of neurofilament protein in progressive supranuclear palsy and multiple-system atrophy compared with Parkinson's disease. *Mov Disord* 13(1):70–77
73. Ye R, Locascio JJ, Goodheart AE, Quan M, Zhang B, Gomperts SN (2021) Serum NFL levels predict progression of motor impairment and reduction in putamen dopamine transporter binding ratios in de novo Parkinson's disease: an 8-year longitudinal study. *Parkinsonism Relat Disord* 85:11–16
74. Utrobičić I, Novak I, Marinović-Terzić I, Matić K, Lessel D, Salamunić I et al (2014) Carpal tunnel syndrome is associated with high fibrinogen and fibrinogen deposits. *Neurosurgery* 75(3):276–285 (**discussion 85**)
75. Panchatcharam M, Salous AK, Brandon J, Miriyala S, Wheeler J, Patil P et al (2014) Mice with targeted inactivation of ppap2b in endothelial and hematopoietic cells display enhanced vascular inflammation and permeability. *Arterioscler Thromb Vasc Biol* 34(4):837–845
76. Ríos-Barrera LD, Sigurbjörnsdóttir S, Baer M, Leptin M (2017) Dual function for Tango1 in secretion of bulky cargo and in ER-Golgi morphology. *Proc Natl Acad Sci U S A* 114(48):E10389–E10398
77. Halbigbauer S, Öckl P, Wirth K, Steinacker P, Otto M (2016) Protein biomarkers in Parkinson's disease: focus on cerebrospinal fluid markers and synaptic proteins. *Mov Disord* 31(6):848–860
78. Thygesen C, Boll I, Finsen B, Modzel M, Larsen MR (2018) Characterizing disease-associated changes in post-translational modifications by mass spectrometry. *Expert Rev Proteom* 15(3):245–258
79. Specht H, Emmott E, Petelski AA, Huffman RG, Perlman DH, Serra M et al (2021) Single-cell proteomic and transcriptomic analysis of macrophage heterogeneity using SCoPE2. *Genome Biol* 22(1):50

Publisher's Note Springer Nature remains neutral with regard to jurisdictional claims in published maps and institutional affiliations.

Authors and Affiliations

Rasmus Rydbirk^{1,2,11} · Ole Østergaard³ · Jonas Folke^{1,2} · Casper Hempel^{4,5} · Brian DellaValle^{2,5} · Thomas L. Andresen⁴ · Annemette Løkkegaard^{6,7} · Anne-Mette Hejl⁷ · Matthias Bode⁸ · Morten Blaabjerg⁸ · Mette Møller⁹ · Erik H. Danielsen⁹ · Lisette Salvesen⁷ · Charlotte C. Starhof⁷ · Sara Bech⁷ · Kristian Winge^{7,12} · Jørgen Rungby^{2,10} · Bente Pakkenberg^{1,6} · Tomasz Brudek^{1,2} · Jesper V. Olsen³ · Susana Aznar^{1,2} 

✉ Jesper V. Olsen
jesper.olsen@cpr.ku.dk

✉ Susana Aznar
susana.aznar.kleijn@regionh.dk

Rasmus Rydbirk
rasmus.rydbirk@bric.ku.dk

Ole Østergaard
ole.ostergaard@cpr.ku.dk

Jonas Folke
jonas.folke@regionh.dk

Casper Hempel
cash@dtu.dk

Brian DellaValle
brian.william.della.valle.01@regionh.dk

Thomas L. Andresen
tlan@dtu.dk

Annemette Løkkegaard
annemette.loekkegaard@regionh.dk

Anne-Mette Hejl
anne-mette.hejl.01@regionh.dk

Matthias Bode
Matthias.Bode@rsyd.dk

Morten Blaabjerg
morten.blaabjerg1@rsyd.dk

Mette Møller
mette.moeller@auh.rm.dk

Erik H. Danielsen
ehdanielsen@biomed.au.dk

Lisette Salvesen
lisette.salvesen@regionh.dk

Charlotte C. Starhof
charlotte.chrom.starhof@regionh.dk

Sara Bech
sara.brynhild.winther.bech.01@regionh.dk

Kristian Winge
Kristian.winge@regionh.dk

Jørgen Rungby
joergen.rungby@regionh.dk

Bente Pakkenberg
Bente.Pakkenberg@regionh.dk

Tomasz Brudek
tomasz.brudek@regionh.dk

¹ Centre for Neuroscience and Stereology, Copenhagen University Hospital, Bispebjerg and Frederiksberg Hospital, 2400 Copenhagen NW, Denmark

² Copenhagen Center for Translational Research, Copenhagen University Hospital, Bispebjerg and Frederiksberg Hospital, 2400 Copenhagen NW, Denmark

³ Novo Nordisk Foundation Center for Protein Research, Faculty of Health and Medical Sciences, University of Copenhagen, 2200 Copenhagen N, Denmark

- ⁴ Department of Health Technology, Technical University of Denmark, 2800 Kgs. Lyngby, Denmark
- ⁵ GLX Analytix ApS, 2200 Copenhagen N, Denmark
- ⁶ Department of Clinical Medicine, Faculty of Health, University of Copenhagen, 2200 Copenhagen N, Denmark
- ⁷ Department of Neurology, Bispebjerg and Frederiksberg Hospital, Copenhagen University Hospital, 2400 Copenhagen NW, Denmark
- ⁸ Department of Neurology, Odense University Hospital, J.B. Winsløvs Vej 4, 5000 Odense, Denmark
- ⁹ Department of Neurology, Aarhus University Hospital, 8200 Aarhus, Denmark
- ¹⁰ Department of Endocrinology, Copenhagen University Hospital, Bispebjerg-Frederiksberg Hospital, 2400 Copenhagen NW, Denmark
- ¹¹ Present Address: Biotech Research and Innovation Centre, Faculty of Health, University of Copenhagen, Copenhagen, Denmark
- ¹² Present Address: Department of Neurology, Odense University Hospital, J.B. Winsløvs Vej 4, 5000 Odense, Denmark